URANIUM POWDER PRODUCTION VIA HYDRIDE FORMATION AND ALPHA PHASE SINTERING OF URANIUM AND URANIUM-ZIRCONIUM ALLOYS FOR ADVANCED NUCLEAR FUEL APPLICATIONS

A Thesis

by

DAVID JOSEPH GARNETTI

Submitted to the Office of Graduate Studies of
Texas A&M University
in partial fulfillment of the requirements for the degree of

MASTER OF SCIENCE

December 2009

Major Subject: Nuclear Engineering

URANIUM POWDER PRODUCTION VIA HYDRIDE FORMATION AND ALPHA PHASE SINTERING OF URANIUM AND URANIUM-ZIRCONIUM ALLOYS FOR ADVANCED NUCLEAR FUEL APPLICATIONS

A Thesis

by

DAVID JOSEPH GARNETTI

Submitted to the Office of Graduate Studies of
Texas A&M University
in partial fulfillment of the requirements for the degree of

MASTER OF SCIENCE

Approved by:

Chair of Committee,	Sean M. McDeavitt
Committee Members,	Ibrahim Karaman
	Lin Shao
Head of Department,	Raymond Juzaitis

December 2009

Major Subject: Nuclear Engineering

ABSTRACT

Uranium Powder Production via Hydride Formation and Alpha Phase Sintering of Uranium and Uranium-Zirconium Alloys for Advanced Nuclear Fuel Applications. (December 2009)

David Joseph Garnetti, B.S. Physics, Florida State University

Chair of Advisory Committee: Dr. Sean M. McDeavitt

The research in this thesis covers the design and implementation of a depleted uranium (DU) powder production system and the initial results of a DU-Zr-Mg alloy alpha phase sintering experiment where the Mg is a surrogate for Pu and Am. The powder production system utilized the uranium hydrogen interaction in order to break down larger pieces of uranium into fine powder. After several iterations, a successful reusable system was built. The nominal size of the powder product was on the order of 1 to 3 μm.

The resulting uranium powder was pressed into pellets of various compositions (DU, DU-10Zr, DU-Mg, DU-10Zr-Mg) and heated to approximately 650˚C, just below the alpha-beta phase transition of uranium. The dimensions of the pellets were measured before and after heating and *in situ* dimension changes were measured using a linear variable differential transducer (LVDT).

Post experiment measurement of the pellets proved to be an unreliable indicator of sintering do the cracking of the pellets during cool down. The cracking caused increases in the diameter and height of the samples. The cracks occurred in greater frequency along the edges of the pellets. All of the pellets, except the DU-10Zr-Mg pellet, were slightly conical in shape. This is believed to be an artifact of the powder pressing procedure. A greater

density occurs on one end of the pellet during pressing and thus leads to gradient in the sinter rate of the pellet. The LVDT measurements proved to be extremely sensitive to outside vibration, making a subset of the data inappropriate for analysis.

The pellets were also analyzed using electron microscopy. All pellets showed signs of sintering and an increase in density. The pellets will the greatest densification and lowest porosity were the DU-Mg and DU-10Zr-Mg. The DU-Mg pellet had a porosity of 14 ± 2.%. The DU-10Zr-Mg porosity could not be conclusively determined due to lack of clearly visible pores in the image, however there were very few pores indicating a high degree of sintering. In the DU-10Zr-Mg alloy, large grains of DU were surrounded by Zr. This phenomena was not present in the DU-10Zr pellet where the Zr and DU stayed segregated. There was no indication of alloying between the Zr and DU in pellets.

DEDICATION

I would like to dedicate this thesis to my family. Without their support I would not have been able to make it this far.

ACKNOWLEDGEMENTS

I would like to thank my committee chair, Dr. McDeavitt, for his guidance and support throughout the course of this research.

I would like to thank the Y-12 plant in Oak Ridge Tennessee and Dr. D. Cecala specifically, for their help in procuring the depleted uranium used in this research.

I would like to thank Kevin Hogan for his help on the MatLAB coding and Ryoji Oinuma for his help on the LabView coding.

I would like to thank Grant Helmreich and Julie Borgmeyer for their help on this project and their microscopy work.

I would like to thank Alissa Stafford for her support in the writing and editing of this thesis.

NOMENCLATURE

TRU	Transuranics
DU	Depleted Uranium
EBR II	Experimental Breeder Reactor II
IFR	Integral Fast Reactor
LVDT	Linear Variable Differential Transformer
SEM	Scanning Electron Microscope

.

TABLE OF CONTENTS

Page

LIST OF FIGURES

FIGURE Page

FIGURE Page

FIGURE Page

LIST OF TABLES

1. INTRODUCTION

The renewed interest in using fast reactors as way to burn the transuranics in used nuclear fuel has lead to this examination of U-TRU-Zr fuel fabrication via powder metallurgical methods. Current methods for U-Zr metal fuel fabrication involve melt-casting technologies that are challenged by the volatility of americium (Am) and neptunium (Np) (Fig 1-1). The the inclusion of Am in advanced fuels is important to the successful transmutation of minor actinides in a fast reactor. Losses of Am during casting will lead to an increase cost to the facility as the material will have to be recovered and then handled appropriately as a waste material [1]. This study was initiated as part of an effort to develop an alternative fabrication method that will not involve significant transuranic losses. It is important to note that recent developments at Idaho National Laboratory[1] have shown that TRU volatility may be overcome by increasing the ambient pressure during injection casting, but powder metallurgy still has significant potential as a fuel fabrication technique.

Injection casting has been the preferred method for metal fuel fabrication for previous fast reactor fuels such as the driver fuel for EBR-II and the demonstration IFR fuel pins. A simplified schematic of injection casting is shown in Fig 1-2, which indicates that the molten fuel alloy is created as a liquid pool in the crucible at ~1500°C, quartz injection molds are inserted into the melt, and the system is pressurized to inject the fuel alloy into the molds creating solid pins. After injection, the filled molds are allowed to cool and then are

---

This thesis follows the style of Journal of Nuclear Materials.

broken away liberating the cast fuel pin that may be machined to specification. Past practice has been to use graphite crucibles coated with a stable oxide powder to minimize interactions between the melt and the crucible. The graphite melt crucible had a dual function as a container and as a susceptor for induction heating. Some carbon contamination from the crucible was always present in the molten alloy. The oxide coating on the casting crucible was applied as a slurry typically containing yttrium , zirconium, or thorium oxides [2].

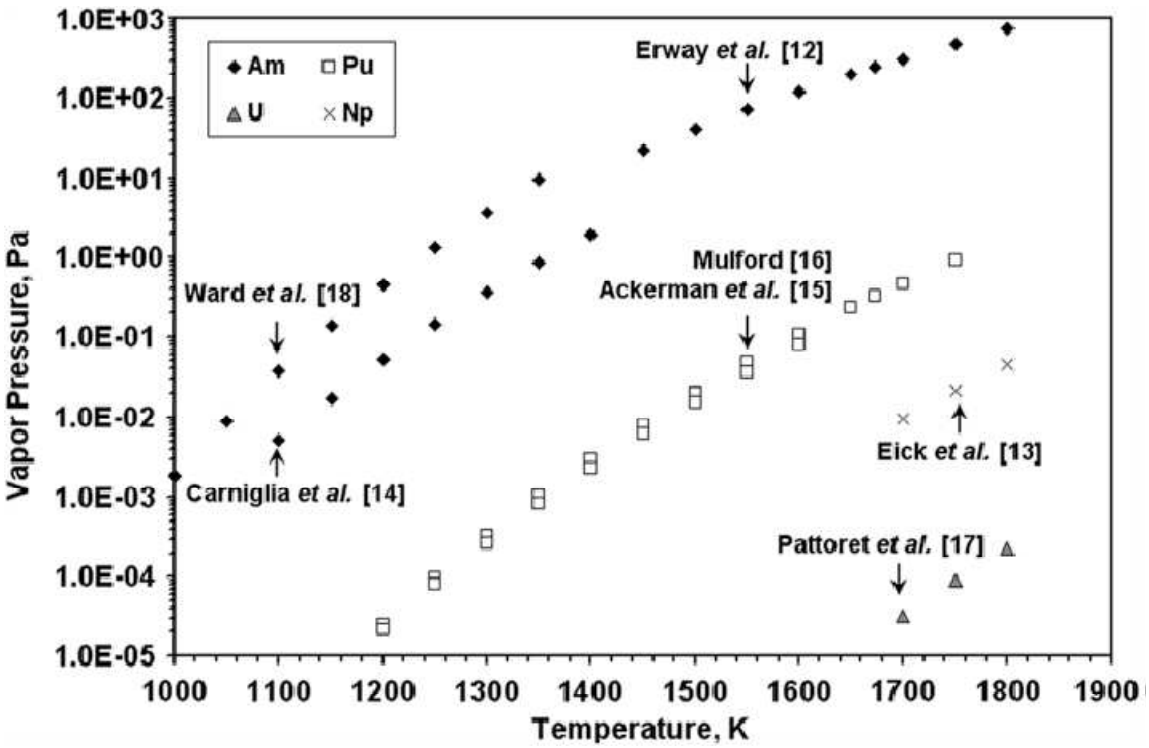

Figure 1-1 Vapor Pressures of the Actinide Metals vs Temperature [1]

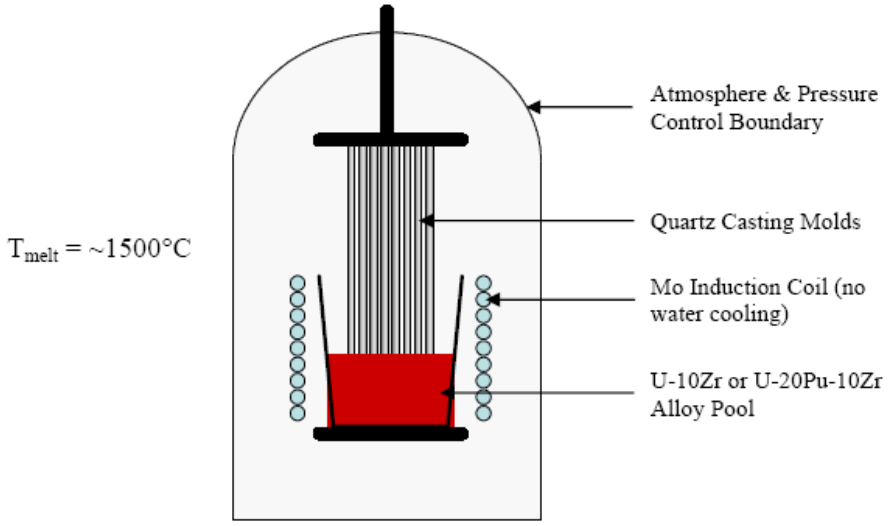

Figure 1-2 Simple schematic of the injection casting process for U-10Zr or U-10Zr-Pu

There are material losses and alloy contamination issues that are inherent in the injection casting process, especially when the higher actinides such as Am are involved in the fuel system. Initial demonstration experiments showed a 40% Am loss from a fuel alloy that had 2.1 wt % Am and 1.3 wt % Np; in this test, the injection casting process was not modified from the nominal U-10Zr methodology [3]. The losses were attributed to evaporation of the volatile contaminates at the casting temperature (1456°C) [3]. Later experiments have shown that these Am losses can be significantly reduced by modifying the casting procedures.

One technique that has been reported involves using a combination of a cover gas and cold trap [1]. A high pressure cover gas was found to reduce Am losses by suppressing Am vaporization. The cold trap is designed to collect any Am that escapes through the high pressure cover gas. This system would be most effective if implemented as a small volume closed system [1]. A small-scale demonstration of this concept was performed with a U-Zr

melt containing 5 wt % Am heated to 1575 K for 5 minutes followed by injection casting. The crucible sides were heated, which made the crucible lid an effective cold trap. Pins were cast with cover gas pressures of 670 Pa and 30 with respective Am losses of 0.3% and 0.006% [1]. This indicates that Am volatility may be overcome and injection casting may be effectively accomplished, but alternative processes are still under development.

The research conducted for this thesis is part of the US Department of Energy's Nuclear Energy Research Initiative (NERI). The goal of NERI is to conduct research that will address key technical issues in the expanding nuclear energy use worldwide. The research in this thesis was conducted under the Advanced Fuel Cycle Initiative (AFCI) category of NERI. The main goal of the research project, which this thesis contributes to, is to develop a method for U-Zr-Pu-Am alloy fabrication that operates at temperatures below 660 °C. The vapor pressures of Am, Np, and Pu are quite low at these temperatures, and therefore volatility losses should not be an issue.

The focus of the research reported in this thesis has been on the development of powder fabrication methods and the initial demonstration of the alpha phase sintering process. Production of fine uranium powder was of the utmost importance for the successful completion of the alpha phase sintering test. A process utilizing the ability to hydride and dehydride uranium was used to produce the uranium powder, 1 to 3 μm sized particles. For reasons of safety and convenience Mg was used as a surrogate in place of Pu. Mg was chosen due to the proximity of its melting point to that of Pu and its relatively high vapor pressure (Mg has a vapor pressure of 0.13 Pa at 500 K). The primary reason for the inclusion of Mg was to simulate the liquid enhanced sintering effect that Pu would have on the pellet. The pellets were made of several different compositions (DU, DU-10Zr, DU-Mg,

and DU-10Zr-Mg). The pellets were all heated to approximately 650 ˚C; some were periodically raised to 700 ˚C and/or 800 ˚C. The pellet dimensions were monitored *in situ* using a linear variable differential transducer (LVDT) as well as physical measurements before and after each experiment. The pellets were cut axially, mounted, and examined using an SEM and digital microscope. Analysis of the LVDT data and SEM imaging indicated sintering of varying degrees in all of the pellets. The research below has created a functioning system and procedures that can produce fine uranium powder for specimen fabrication and it has provided a solid base upon which a larger test matrix can establish the behavior of the sintering and liquid phase sintering methods.

2. BACKGROUND

The focus of this section is to provide a survey of the relevant physical phenomena and technical context that underpins development activities described in the following sections. Section 2.1 provides a brief summary of the mechanisms and models that describe sintering. Section 2.2 provides a summary of the properties of alpha phase uranium and the uranium-zirconium binary system. Section 2.3 summarizes previous work concerning powder production via uranium hydration.

2.1 Sintering

Sintering is the physical process where a form comprised of compacted particles (e.g., powder) is transformed into a dense structure at elevated temperatures through diffusion controlled mechanisms. The process involves the heating of the form and may involve the application of external pressure to the specimen or the addition of a small amount of liquid phase materials [4]. The main driving force of sintering is the reduction of surface area to minimize surface energy within the body. Points of contact between powder particles will initially have a local radius of curvature near zero, which creates a near-infinite driving force for diffusion into that point to form a “neck” or bridge between the particles. There are six different sintering mechanisms outlined in Fig. 2-1 that are typically observed in powder metallurgy and ceramics: surface diffusion; lattice diffusion (from the surface); vapor transport; grain boundary diffusion; lattice diffusion (from the grain boundary); plastic flow [5].

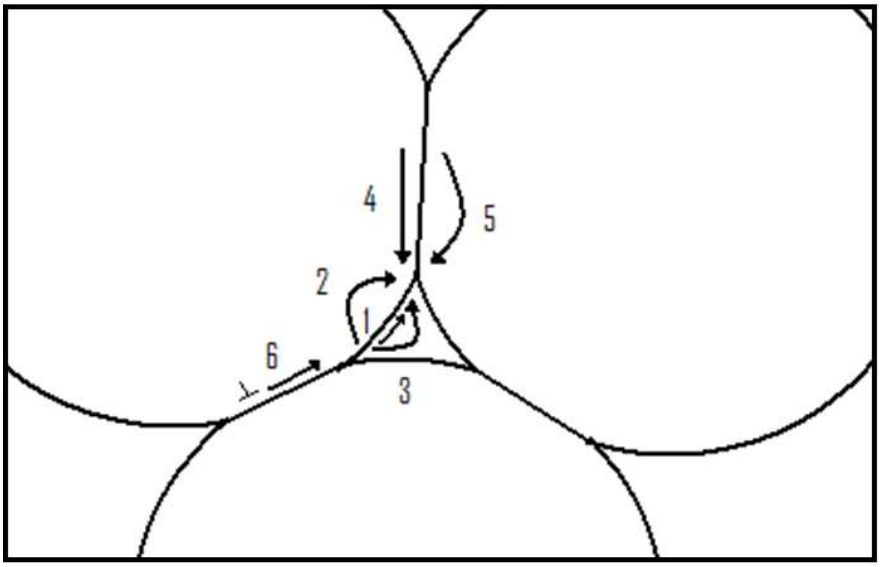

Figure 2-1 Various sinter mechanics: 1 Surface diffusion; 2 Lattice diffusion (from the surface); 3 Vapor transport; 4 Grain Boundary diffusion; 5 Lattice diffusion (from the grain boundary; 6 Plastic flow

As the particles come together by whatever mechanism dominates, the internal void space begins to close and internal porosity is formed. As sintering progresses, there is a significant change in the morphology of this porosity. Initially, pores change from irregular shapes into spherical shapes, again to minimize surface energy effects, and then the volume fraction of the porosity is reduced as the diffusive driving force continues to drive the body toward higher density. Over time, the radius of the pores decreases until an equilibrium condition is reached where the internal pore pressure, p, is balanced by the surface energy "pressure" according to

$$p = \frac{2\gamma}{r}$$

where γ is the surface energy, and r is the radius of curvature for the pore [4]. At this point, shrinkage of the specimen stops. If the external pressure of the body is changed, swelling or densification may occur in order to achieve a new equilibrium [4].

The sintering rate is defined as the rate at which the material densifies and it is often modeled in terms of volumetric strain rate.

$$\text{Sintering Rate} = \frac{d}{dt}\left(\frac{\Delta V}{V_o}\right)$$

where V is the overall volume of the form being sintered. While the total amount of sintering can be easily measured by recording the volume and weight of the specimen before and after heating, it is valuable to know the rate of sintering during the heating process. If the sintering rate is continuingly measured, one can calculate the process activation energy between two different temperatures. The rate of sintering for a powder pressed pellet can be measured in several ways. Two methods which are utilized in this experiment are the measuring of density before and after sintering and the continuous measurement of linear shrinkage [6].

Linear shrinkage was measured using a linear variable differential transducer (LVDT). It is assumed that the volume change in the sample was isotropic, leading to the following equation [6]:

$$\frac{\Delta V}{V_o} = 1 - \left(1 - \frac{\Delta L}{L_o}\right)^3 \approx 3\frac{\Delta L}{L_o}$$

where $\frac{\Delta V}{V_o}$ is the volumetric strain, and $\frac{\Delta L}{L_o}$ is the linear strain. One can also estimate the post sintering volume of the specimen from Y (where $Y = \frac{\Delta L}{L_o}$).[6].

$$V_S = V_G \frac{1}{(1+Y)^3}$$

where V_S is the sintered fractional solid volume and V_G is the green volume.

2.2 Alpha Phase Uranium

2.2.1 Uranium/Alpha Phase Uranium

Uranium may exist in three allotropic phases named α, β, and γ. The alpha phase is stable from low temperatures up to 667°C and has a complex orthorhombic structure [7]. The beta phase has a complex tetragonal structure and is stable in the temperature range of 667 °C to 772 °C. The gamma phase is stable from 772 °C up to the melting point, 1132°C and has a body centered cubic structure. Alpha phase uranium has a theoretical density of 19.04 g/cc at 25 °C [8]. The orthorhombic structure has the following lattice parameter dimensions at 25 °C: a=2.8541 Å, b=5.8541 Å, and c=4.9563 Å [7] [8]. These values are more precise that the older values shown in Fig. 2-2.

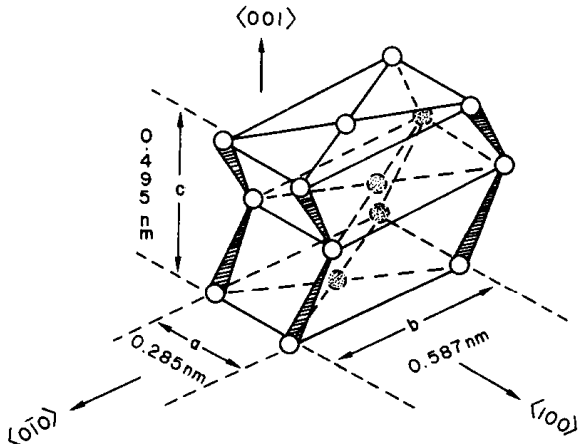

Fig. 2-2 Alpha phase uranium, orthorhombic crystal lattice [7]

At the advent of nuclear energy, pure uranium metal was one of the first fuel forms investigated. Uranium metal has the technical benefits of being of a higher density and having a higher thermal conductivity than oxide fuel. However the well documented swelling of the fuel in the alpha phase of pure uranium metal caused it to be an unusable fuel form [9]. However the swelling issues associated with irradiation "tearing" were overcome through alloying with elements such as zirconium, molybdenum, and other noble metals; uranium zirconium alloys have been used for several fast reactor systems in the past 50 years [10] [11]. During testing of irradiated fuel it has been noted that there is a recovery driven reduction of tearing above 550˚C. The recovery driven reduction has lead to a decrease in the linear shrinkage in some cases [11]. This recovery mechanism has been noted in the work of Burke, Pugh, and McDeavitt [9] [10] [12] [13].

Previous work reported by Chiotti, et al. [14] provides additional relevant experience with uranium powder metallurgy that has been of great benefit to this current project. In this work, a hydride-dehydride process was studied extensively to evaluate the mechanisms of UH_3 formation and decomposition. This work is especially relevant to the powder fabrication method development discussed in Sections 3.1 and 4.1. However, in the midst of this previous study, Chiotti reported the observation of alpha-phase sintering during dehyriding experiments where UH_3 was placed under a vacuum and brought to temperatures above 300°C [14]. As the hydrogen was disassociated from the uranium, loose sintering of the uranium powder was evident because the powder came out of the experiments in solid, but porous "chunks."

All of the observations noted above can be taken together as evidence that uranium has significant diffusive mobility in the alpha phase at temperatures just below the alpha-beta phase transformation temperature.

2.2.2 Alpha Phase Uranium in Uranium Zirconium Alloys

Figure 2-3 shows the binary U-Zr phase diagram [15]. As noted in Section 2.2.1, zirconium is a commonly-used alloying element with uranium in nuclear fuels for fast reactor systems. Pure zirconium exists in two phases: 1) a hexagonal phase stable up to 862˚C (α) and 2) a body center cubic phase stable from 826˚C to the melting point1852˚C (β). In the U-Zr binary system an intermetallic δ-UZr_2 phase is formed bellow 617 ˚C. The δ phase consists nominally of UZr_2 and has a ω-type structure [16] [17]. The U-Zr also contains a γ phase which exhibit full mutual solubility of U and Zr. However the uranium β phase can only dissolve a maximum of 0.4 Wt% of Zr (at 693˚C) and the uranium α phase can dissolve a maximum of 0.2 Wt% of Zr (at 662˚C) [16]. The γ uranium phase has the highest solubility limit for Zr as it shares the same structure, BCC, as the β zirconium phase. Also the alpha beta phase transition line is lowered to 662 ˚C in the U-Zr system.

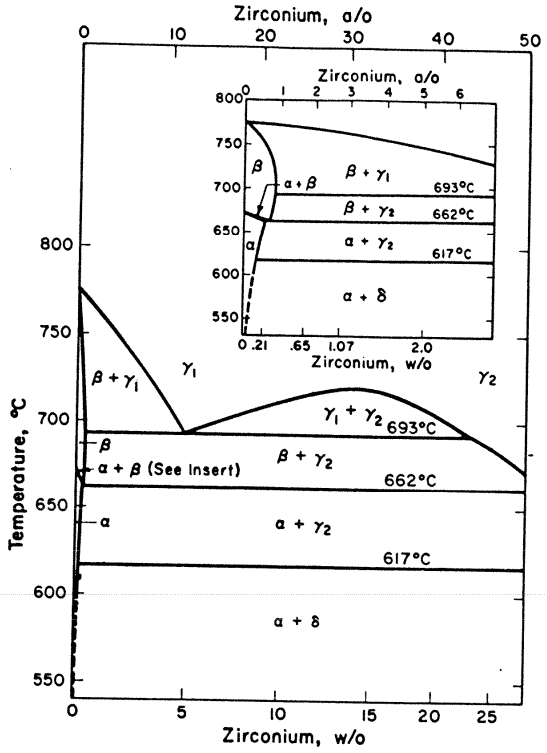

Fig. 2-3 Uranium-Zirconium Phase diagram, with insert [15]

In the previous work of McDeavitt and Solomon [12] [13], the sintering of dehydrided uranium zirconium alloys was observed at temperatures as low as 400°C. and continued until the alpha-beta phase transition line is reached. There was an increase from approximately 44% theoretical density to 49% theoretical density before the alpha beta phase transition line, Fig. 2-4 [12]. The increase is density is evidence of sintering of the specimens during the alpha phase. As the research at the time was not focusing on this phenomenon, it was noted but not thoroughly examined.

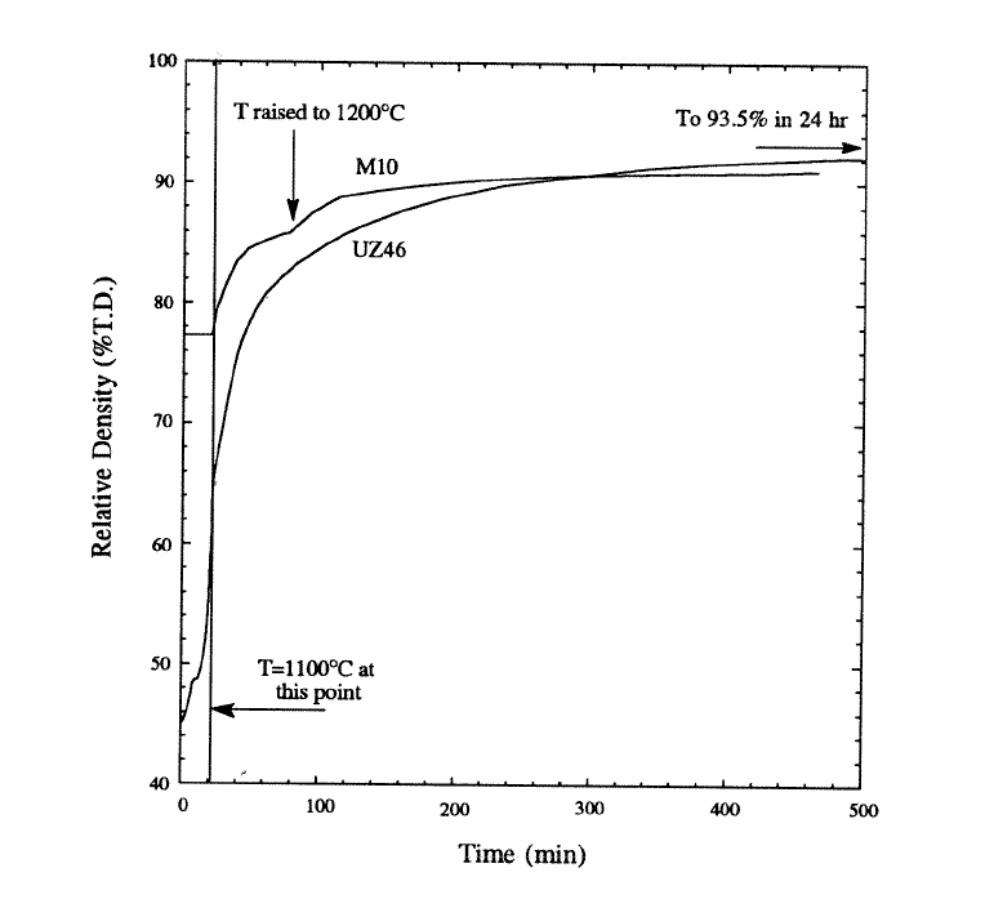

Fig. 2-4 Shows an increase in TD before alpha beta phase transition [12]

2.3 The Uranium Hydride/Dehydride Process

One method that has been previously used to produce fine uranium powder with low oxygen contamination is known as the hydride/dehydride process. This process has the ability to transform pieces of uranium into a high purity fine powder [18].

2.3.1 Uranium Hydride

Uranium Hydride (UH_3) is formed through the following reversible reaction [18]:

$2U + 3H_2 \rightleftharpoons 2UH_3$.

When the reaction takes place with solid uranium metal slugs, it causes the complete destruction of the original structure of the metal [19] due to the large difference in density of uranium metal (19.04 g/cm^3) and UH_3 (10.9 g/ cm^3) [20]. The reaction leaves behind a fine powder that is of black/dark brown color with nominal particle sizes ranging from less than 1 μm up to ~10 μm (approximately -400 mesh) when the reaction is carried out at a temperature of 225 °C [11] [19]. The three principle factors affecting the rate reaction (assuming no oxidation layer is present on the uranium surface) are the surface area of the sample, temperature, and the hydrogen pressure in the reaction chamber [14].

Hydrogen will interact with uranium at temperatures below 150°C, however the reaction reaches maximum efficiency at approximately 225°C, Fig. 2-5 [11] [19]. An induction period has been noticed when hydriding uranium metal at lower temperature. This is most likely caused by the presence of an oxide layer on the uranium metal surface [19]. In cases where there is an oxide layer on the uranium specimens, it has been recommended to initiate the reaction over 300°C; this leads in an increase in the hydrogen diffusion through the oxide layer on the uranium [11]. However, hydriding at temperatures above 300 °C can lead to some sintering of the uranium hydride powder [11].

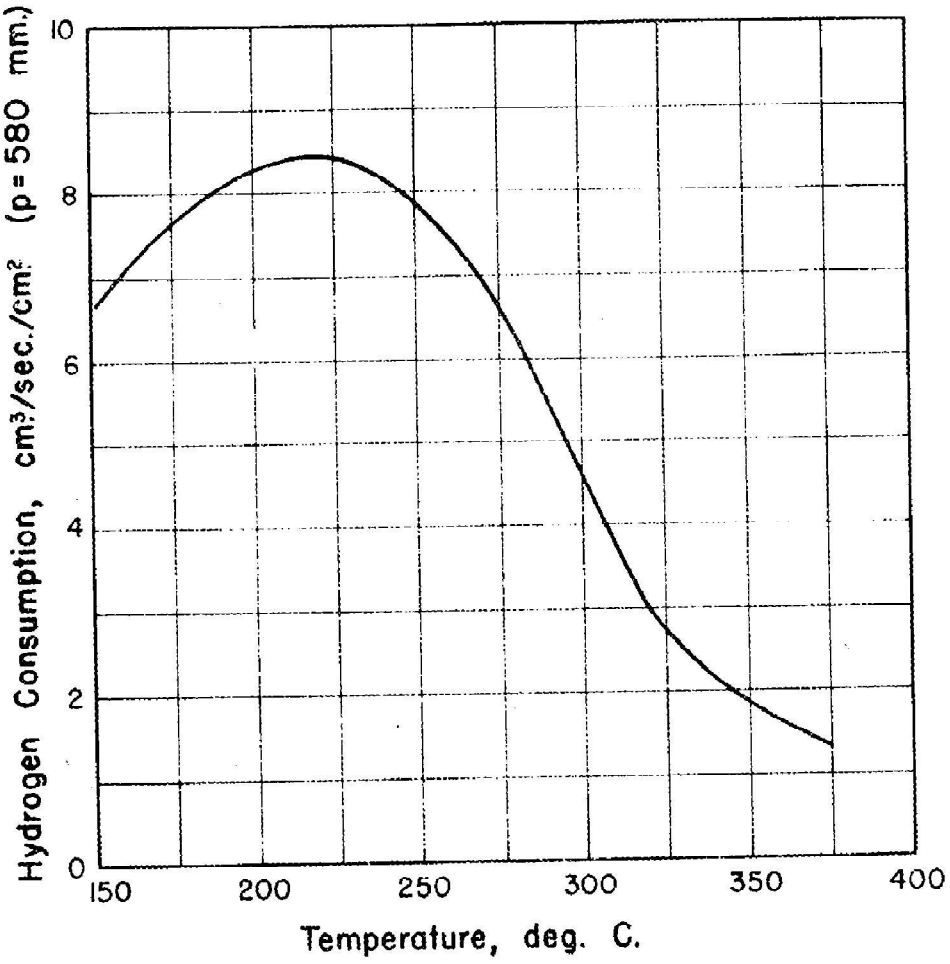

Fig. 2-5 Hydration rate of uranium at constant pressure [14]

2.3.2 Dehydriding Uranium

UH_3 disassociation at atmospheric pressures requires temperatures above 430 °C, Fig. 2-6 [14]. This process can be expedited by heating the uranium hydride in a vacuum. The stabilization of the pressure in the reaction vessel is an indicator that the hydrogen has "completely" disassociated. The uranium metal left behind is in the form of a high purity powder with an average size of a less than 40 μm [11] [18]. During the dehydriding step,

there is a tendency for the powder to sinter into aggregate particles. This sintering becomes noticeable above 300°C. However, these aggregates can be easily broken down by mechanical milling when the dehydriding temperature is kept below ~400°C [14].

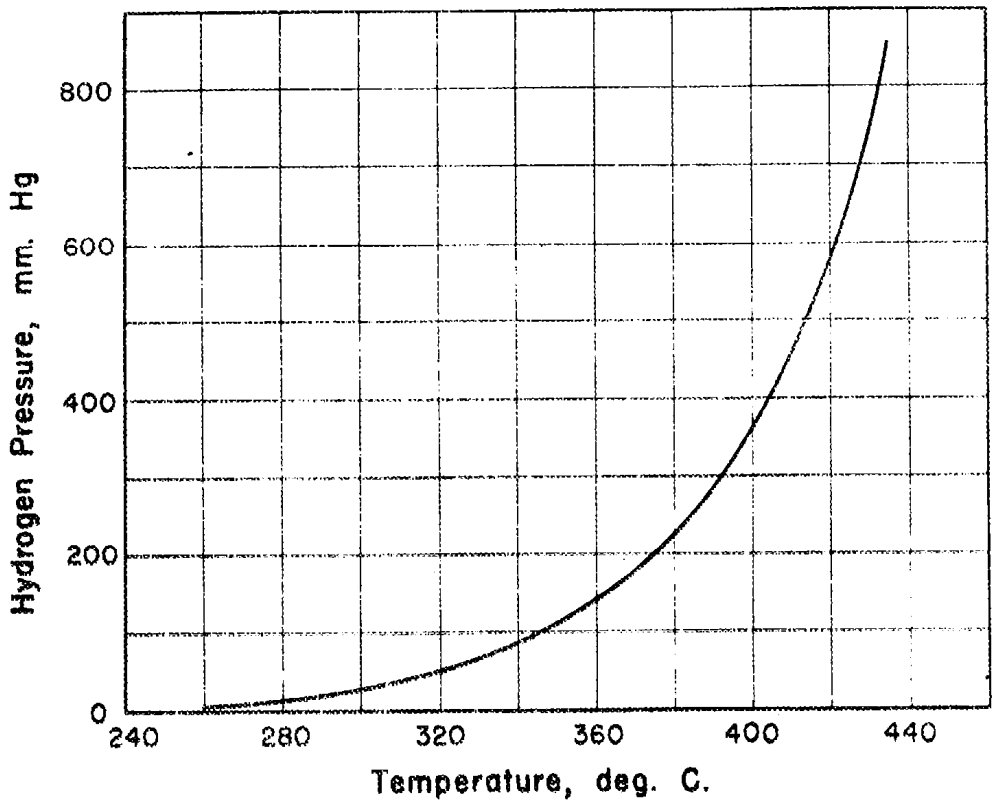

Fig. 2-6 Hydrogen disassociation rate at various temperatures [14]

2.3.3 Uranium Oxide Removal with Nitric Acid

As previously noted, an oxide layer will create a barrier to the diffusion of hydrogen throughout the sample and slow down the hydride formation [19]. An oxide layer may also cause oxygen contamination in the UH_3 and uranium metal powder produced. Therefore it is necessary to remove any oxide layer from the uranium chips as completely as possible.

In order to remove the oxide layer, the uranium chips are placed in a nitric acid solution bath. In previous studies a solution of 25% nitric acid by volume was sufficient for the removal of the oxide layer of 80 mesh uranium metal spheres [12]. The reaction takes places rather quickly, and if the uranium is left in the nitric acid too long the solution will heat up. This will lead to the re-formation of the oxide layer on the uranium [12].

3. EXPERIMENTAL DESIGN AND PROCEDURES

This section describes the three main components of the experimental systems and procedures developed for this thesis. None of the systems described were in existence at the onset of this research, so a major portion of the work reported here was in the establishment of this equipment to the point that the procedures could be performed to meet the research objectives. The three main sections of this section describe the methods and equipment established to perform for the production of uranium metal powder (Section 3.1 & 3.2), the generation of pressed pellets using metal powder mixtures (Section 3.3), and sintering the pressed pellet (Section 3.4 & 3.5). For all three of these operations, great care was required to minimize oxygen contamination of the metal powders. Therefore, nearly all of the experiment takes place in a large inert argon atmosphere glovebox, Fig. 3-1. The operations that were not performed inside of the glovebox are the initial acid washing of the uranium chunks for powder production and the preparation of the experimental samples for SEM and digital microscope analysis. The acid wash step was performed inside of an argon (Ar) atmosphere glovebag and the metallurgical sample preparation was performed in air and both operations were performed in a fume hood.

Fig. 3-1 Inert atmosphere glovebox, primary location of the experiments

3.1 Powder Production Experimental Design

High purity uranium metal powder is highly reactive with air and is not readily available for purchase. Therefore, a reliable uranium powder production method was needed in the laboratory to create the powders required for pressing and sintering. The method selected involves the conversion of uranium metal slugs into uranium hydride powder through vapor phase synthesis and the decomposition of that powder into metal by thermal decomposition; this method is named the hydride/dehyride process. The uranium used in this experiment was obtained from the Y-12 plant at Oak Ridge National Laboratory. The uranium was in the form of rectangular metal chunks weighing approximately 10 to 30 g. The chunks had a black oxide layer which needed to be removed to expose the metal surface

before the uranium could be hydrided. A hydride/dehdyride system was installed in and around the glovebox; a basic schematic of the final system is shown in Fig. 3-2.

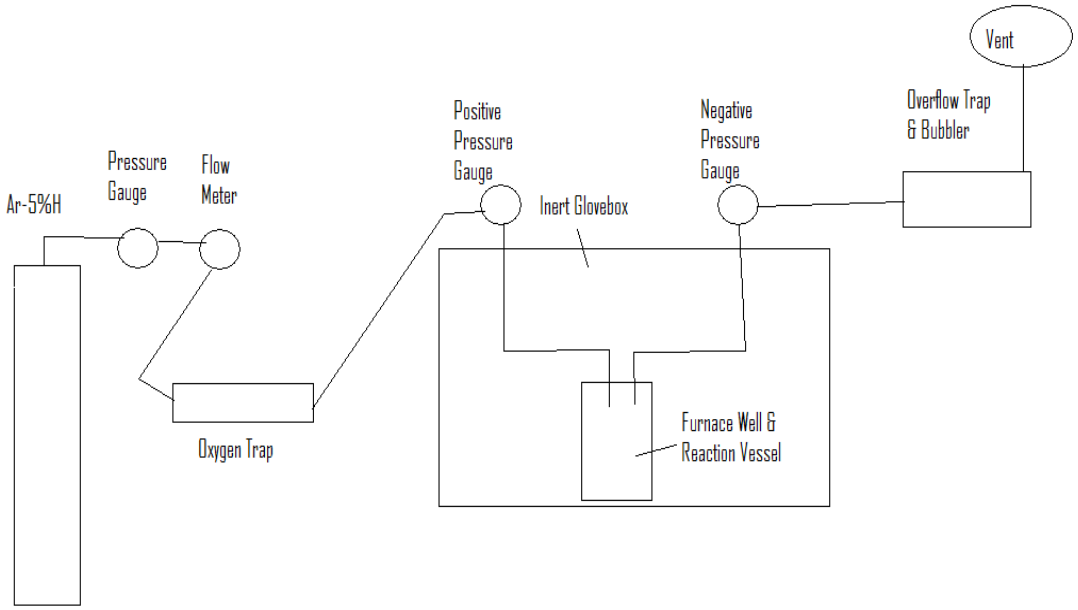

Fig. 3-2 Schematic of the Hydride/Dehydride System

3.1.1 Process Gas Flow

The process gas came from two separate sources, a gas cylinder of welders-grade Ar gas and a gas cylinder of Ar-5%H_2. The gas flow system went through several iterations. Originally the system only used the process gas, Ar-5%H_2, and was monitored by a precession pressure gauge and 10 psi relief valve. The gas line was connected to the east airlock of the glovebox. This design was used for hydride experiments 1 through 4. Later

the gas line was moved from the airlock to the furnace well of the glovebox and attached to a hydride/dehydride reaction vessel that was inserted into a heated furnace well within the glovebox. This design was used for hydride experiments 4 onward. The gas flowed from the furnace well out of the glovebox to an overflow trap and then a silicon oil bubbler. This was done to prevent contaminants from entering the system. The gas then flowed into a fume hood where it was vented to the atmosphere. At this time the gas cylinder containing Ar was added, as it was necessary to fill the furnace well with Ar before removing the reactions vessel. This was done to avoid exposing the glovebox atmosphere to H_2. Next a Ti getter, housed in an alumina tube, was added to the gas flow design. This Ti getter was designed and used in previous Zircaloy hydriding experiments by Adam Parkinson [21]. With the Ti getter a flow meter, pressure gauge and 5 psi relief valve was added to system. In the final iteration the Ti getter was replaced by a commercial bought oxygen and moisture trap. The 5 psi relief valve was removed. All other components of the system remained unchanged. A schematic of the final gas delivery system is shown in Fig. 3-3.

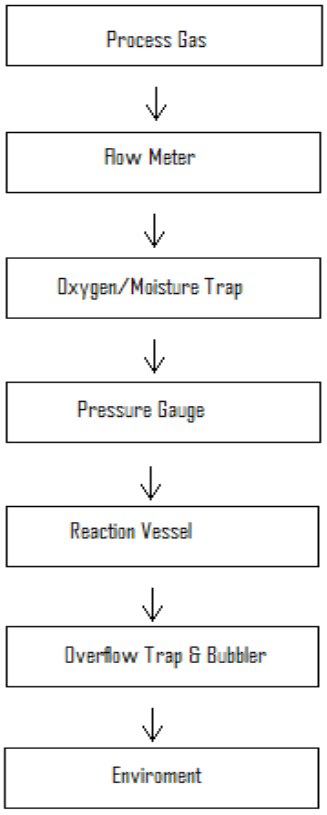

Fig. 3-3 Schematic of the process gas flow path

3.1.2 Titanium Getter/Oxygen and Moisture Trap

The titanium getter, Fig. 3-4, was added during hydride experiment 8, in order to eliminate contaminants from the gas delivery system (N_2, O_2, H_2O). The Ti getter consisted of a 1 5/8 in diameter alumina oxide tube with 350 W Watlow furnace around it. The tube was filled with Ti sponge in the heated region only. This was done to avoid forming TiH_2 on the periphery of the getter furnace [21]. The Ti sponge was kept at a temperature of approximately 1025°C. At this temperature the Ti would not hydride or form a eutectic with the stainless steel cage.

A cage was fabricated to keep the Ti sponge in the heated region. The cage consisted of a 64x64 stainless steel mesh formed into a cylinder with a diameter of approximately 1 3/8 in. On one end of the cylinder a hole was cut to allow an alumina tube to enter the sponge. The alumina tube was used to protect the thermocouple from interacting with the Ti sponge. The cage was then placed in the 1 5/8 diameter alumina tube, filled with Ti sponge, and the thermocouple was inserted.

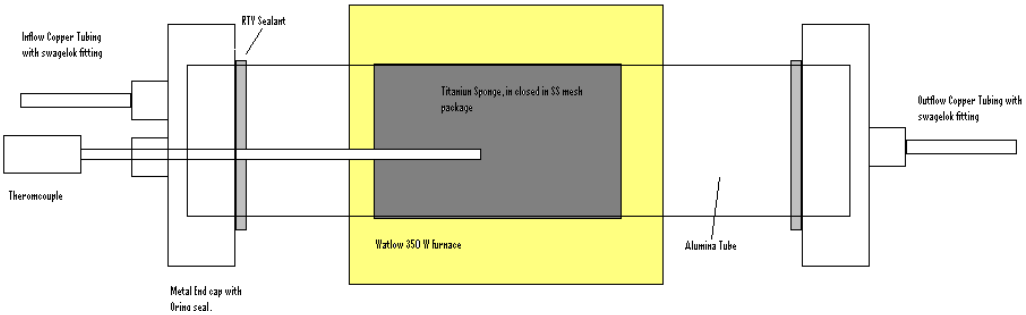

Fig. 3-4, Diagram of Ti Getter

Finally the Ti getter was replaced by an oxygen trap (Alltech Big Oxygen Trap Model 7217) and moisture trap (Alltech Big Moisture Trap Model 7211) during hydride experiment 13. Both of these traps were designed to handle a maximum pressure of 250 psig. The oxygen trap was designed to limit the oxygen to less than 100 ppb and the moisture trap was designed to less than 100 ppb. In practice when placed in series and connected to an Ar gas cylinder with an oxygen level of approximately 14 ppm the traps lowered to the oxygen level to approximately 1.5 ppm and the moisture level was 1 ppm. This oxygen level should have a negligible effect on the hydride system.

3.1.3 Hydride/Dehydride Reaction Vessel

As with the gas delivery system the hydride/dehydride reaction vessel went through several iterations. The original design consisted of a furnace system contained within the east airlock of the glovebox, Fig. 3-5. A 350 W Watlow furnace was placed in the center of a stainless steel pot, diameter 20.32 cm (8 in), with the insulation surrounding it. The samples were contained within a Y_2O_3 crucible which in turn was placed in the furnace. The top gasket of the airlock had a Conax Buffalo feedthrough installed. The feed-through consisted of 6 wires two 12AWG and four 24 AWG thermocouple wire. The 12 AWG wires were used to power the furnace while the thermocouple wiring was attached to two K-type thermocouples. One thermocouple was used to take reading from the Y_2O_3 crucible while the other thermocouple took readings from the insulation region of the system. The furnace reached temperatures upwards of 450°C while the temperature of the airlock walls remained near room temperature. This system was used for hydride experiments 1 through 4. This setup however was found to be inadequate due to O_2 contamination from outside of the system.

Fig. 3-5 Left:Hydride/Dehydride furnace original setup. Right: East airlock with Conax Buffalo electrical feedthrough

The reaction vessel was then moved to inside of the glovebox to eliminate the possibility of contamination from outside the system. The reaction vessel consisted of a dipper device with a rubber stopper on top. A simplified schematic is shown in Fig. 3-6.

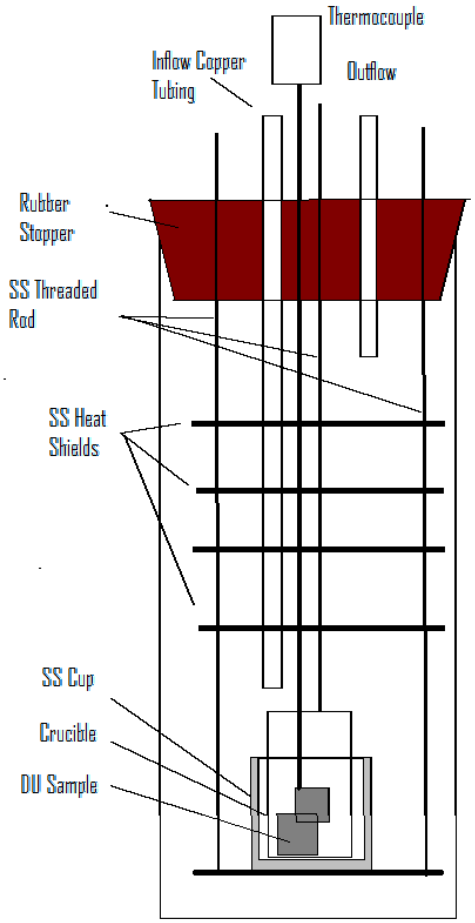

Fig. 3-6 Schematic of Hydride/Dehydride Reaction Vessel

The reaction vessel assembly was fabricated using 1.875 inch diameter 304 stainless steel discs connected by 24 inch long ¼ in diameter 316 stainless steel threaded rod. On the bottom plate a cup was fabricated from 304 stainless steel. The cup had a diameter of 2.3 cm. The cup was affixed to the bottom by a ¼ in screw. An alumina crucible (V=10mL,

OD =22 mm, H = 33mm), which contained the sample, was placed inside of the cup. A high temperature resilient rubber plug was located at the top of the vessel; top diameter 2.48 in, bottom diameter 1.97 in. The opening to the furnace well had a diameter of approximately 2 in. The rubber plug had two sections of ¼ in copper tubing going through it. The center piece of tubing (inflow) ran the length of the dipper while the other piece of tubing (outflow) only protruded approximately 3 cm into the well. The three pieces of threaded rod also protruded from the top of the rubber stopper. The threaded rods and tubing were affixed in place using Torr Seal. This created a gas tight seal with the ability to withstand a rough vacuum, Fig. 3-7. When in use, the gas flow system described above was attached to the inflow and outflow tubing of the reaction vessel. The reaction vessel was kept in place during the experiments by placing weight on top of the stopper to counteract the increase in pressure of the furnace well. This system was used successfully for hydride experiments 5 and onward, but a better design is required for future activities. The Ti getter was used in conjunction with the system for experiment 8 through 12. From experiment 13 onward the oxygen and moisture traps were used in place of the Ti getter.

Fig. 3-7 Hydride/dehydride reaction vessel inside of large glovebox

3.1.4 Nitric Acid Washing of Samples

The depleted uranium samples had an oxide layer which had to be removed before the experiments could take place. The oxide layer was removed through acid washing using a 35% volume nitric acid solution. The nitric acid washing station was setup within a glovebag which was purged with Ar gas. The glovebag (Glas-Col Model X-27-17) was located within a fume hood, Fig. 3-8.

Fig. 3-8 The Depleted Uranium Washing Station

3.2 Powder Production Experimental Procedures

3.2.1 Sample Preparation

The samples were weighed inside of the glovebox using an AL-204 Balance. The due to the fluctuations in glovebox pressure balance had an accuracy of 0.0005 g, the samples were weighed 5 times each given these measurements 0.0002 g accuracy. The samples were then either cut down to a manageable size using a diamond saw and the pieces reweighed individually or taken directly to the nitric acid washing station. The samples were washed in the nitric acid and then rinsed with water over the beaker containing the 35% volume nitric acid solution. The samples were placed in the nitric acid solution for 10-15

minutes or until the oxide layer was removed. There was a visible reaction between the nitric acid solution and the depleted uranium samples. Bubbles would begin to form on the surface of the samples and sometimes the nitric acid solution would change from clear to yellow in color. Once the black oxide layer was removed the depleted uranium sample was a dull silver color with a tinge of gold. The samples were then rinsed with 190 alcohol over a separate beaker. The samples were then immediately taken into the glovebox in order to limit oxidation of the samples post wash.

The samples were reweighed and placed in the crucible of the hydride reaction vessel. The vessel was then placed into the furnace well and connected to the inflow and outflow piping.

3.2.2 Hydride Reaction

After the reaction vessel was connected the gas flow lines the glovebox inlet and overflow trap outlet valve were closed, the vessel was evacuated and a rough vacuum was held for five minutes to remove the original atmosphere in the reaction vessel. The gas flow was changed to Ar-5%H_2 and reaction vessel was pressurized. The sample was kept under Ar-5%H_2 flow while being heated to the set temperature. During the initial experiments the reaction vessel was placed under vacuum for time period of 15-30 minutes periodically after temperature was reached, thus dehydriding the sample. This was done to expose a fresh surface for a hydride reaction and to facilitate the breaking up of the uranium pieces. In later experiments it was determined that this was an extraneous action and therefore was not continued.

After the uranium pieces were sufficiently hydrided the reaction vessel was once again evacuated. The vessel was held at temperature and under vacuum to allow the

hydrogen to completely disassociate for the uranium. The pressure of the system was monitored once the temperature reached 350˚C. During disassociation, the pressure in the vessel would increase for vacuum to approximately 7 Pa and return to vacuum once disassociation was complete. Once the majority of the disassociation reaction was completed the vacuum pressure would return to its previous level. The well was held under vacuum for an additional 15 minutes to insure full disassociation of the hydrogen before cooling began. After the dehydridng was complete and the well sufficiently cooled, the vessel was repressurized using argon gas. The uranium powder was removed from the crucible and then weighed.

Upon removal from the reaction vessel the uranium metal powder was loosely sintered. The sintered pieces were first broken apart by physical shaking the jar the uranium was held in. Then the broken pieces were placed in a stainless steel mortar and pestle were the pieces were ground into a powder. That powder was then place in in a horizontal vibratory mill with the commercial name “Wig-L-Bug” (Model # 3110B) with or without the addition of a stainless steel bearing. The powder was shaken until a fine powder was obtained. The remaining pieces of uranium, which were not hydrided, were removed and used in later hydride experiments. The nominal particle size of the resulting powder was on the order of 1 to 3 μm.

3.3 Pellet Pressing Design and Procedures

The pellets were pressed in a double action punch and die with a pellet diameter of approximately 9.5 mm (0.375 in). The die was fabricated first. Then the punches were fabricated by incrementally turning down the punch radius, to insure a tight fit. Initially the

dies and punches were fabricated from 303 stainless steel, due to the anti-galling and machineable qualities of this alloy. After the first sintering experiment it was determined that the 303 punches could not handle the necessary force without drastically deforming. From sintering experiment 2 the punches were fabricated from H13 tool steel. The H13 punches were heated treated and tempered after fabrication. The pellets were pressed inside the glovebox using a hydraulic press (Caver Laboratory Press Model C).

After weighing the uranium and zirconium powder for the pellet the powders were placed in a stainless steel container. They were then mixed until homogenous using the Wig-L-Bug mixing device. The homogenously mixed powder was then poured into the die with bottom punch in place. The punch and die was then placed on the hydraulic press and the top punch was inserted. In an effort to limit contamination of the pellets no lubrication was used with the punch and die. The pellets were pressed with a maximum load of 15,000 lbs over the 9.5 mm (0.375 in) diameter pellet or approximately 135,000 psi. The pressed pellet was then removed and either placed directly in the furnace well and sintered or placed in sealed container and stored for a later experiment.

3.4 Alpha Phase Sintering Experimental Design

The alpha phase sintering experiments made use of the same furnace as well as the previously mentioned hydride experiments, Fig. 3-9. A reaction vessel was constructed using 316 stainless steel threaded rods, 304 stainless steel heat shields, and a fabricated 304 stainless steel cup, Fig. 3-10. The cup was a fixed to the bottom heat shield via ¼ inch screw. The inner diameter of the cup was 0.90 inches. The alumina crucible was placed inside on the cup and held the pellet during the experiments. The heat shields had a

diameter on 1.875 inches. The heat shields were attached to the threaded rod using hex nuts and each had a ¼ inch hole located in the center. The top plate had a diameter of 2.5 inches. This rested over top of the opening of the furnace well and allowed the rest of the device to hang from that point. Through the center hole a stainless steel rod could be placed. At the top of this rod, the magnet for the LVDT was be affixed to enable monitoring of dimension changes in the specimens. The bottom of the stainless steel rod was covered with a yttrium oxide sheath to prevent interaction with the pellet.

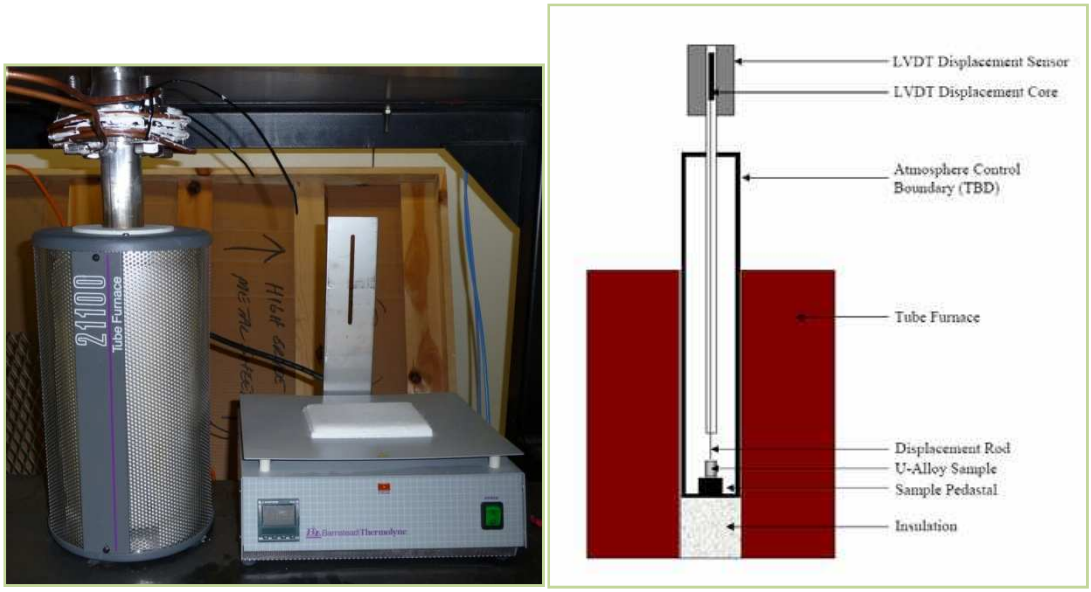

Fig. 3-9 Left: The furnace well and furnace used in the sintering rate and powder production experiments. Right: A simplified schematic of the sintering rate experimental setup

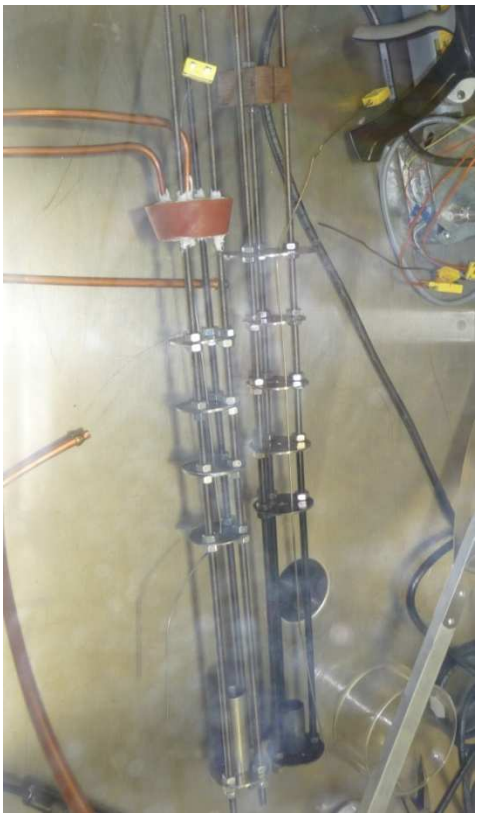

Fig. 3-10 The alpha phase sintering experiment reaction vessel (right) lying next to the hydride reaction vessel (left) on the glovebox floor.

The LVDT was held in place using a carved wooden block which could be tightened or loosened around the LVDT by turning a small screw. The design of the LVDT allows for no interference from frictional forces as it moves freely and does not come into contact with the walls of LVDT, Fig. 3-11.

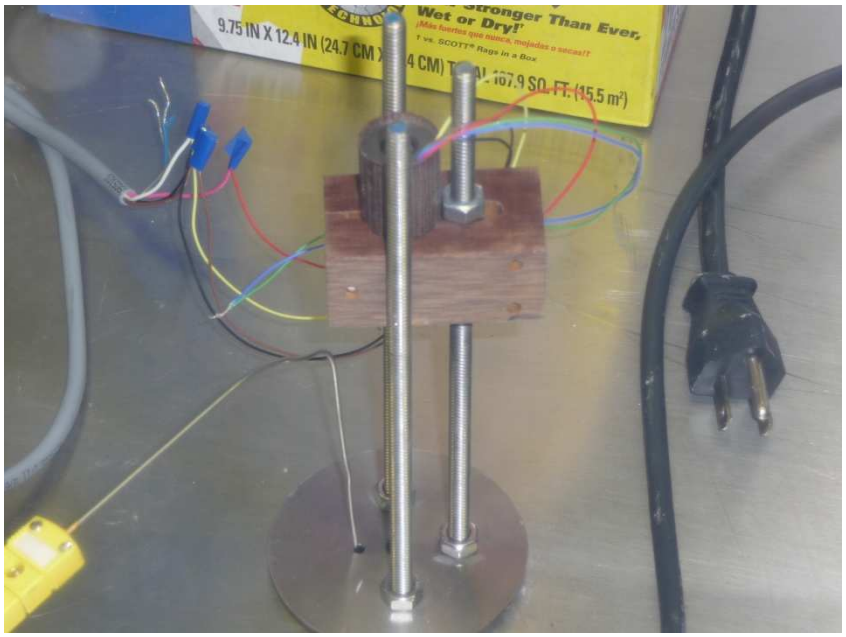

Fig. 3-11 The LVDT with magnet inserted held by the reaction vessel

3.5 Alpha Phase Sintering Experimental Procedures

The pressed pellet was either stored in a sealed container or immediately used in a sintering rate experiment. Before being placed in the furnace well the pellets were weighed using the balance. The diameter and height of the pellets were measured using calipers with an error or 0.0127 mm, the measurements were taken 5 times for each dimension giving a total error for these measurement 00057 mm. The pellets were only handled with tweezers and never came in contact with the gloves in order to prevent contamination of the samples. The pellets were then placed in an alumina crucible which was placed into the cup at the end of the holder.

The LVDT was used to monitor the sintering rate of the pellet. The LVDT magnet was attached to the end of a threaded rod and the rod inserted in the center of the holder. The yttrium oxide sheath was placed over the end of the rod and the sheathed rod was

allowed to rest on top of the pellet. The holder was then placed into the furnace well. The LVDT was then positioned such that the magnet was completely surrounded. Also the magnet was placed towards the upper end of the LVDT so that there would be less chance of the magnet lowering outside the bounds of the LVDT during the experiment, thus stopping the differential voltage signal. The LVDT was then secured by tightening the wooden holder around it.

The k thermocouple and the LVDT were connected to two display units which in turn were connected to a DAQ (National Instrument USB 6029 DAQ). The signals were compiled using the data acquisition program LabView 8.6. The rough data was exported into a Matlab program for analysis.

4. RESULTS

The first section of this section, Section 4.1, describes the results from the uranium hydride/dehydride experiments performed to develop the process to produce clean, fine uranium powder (referred as the powder production experiments). Section 4.2 describes the experiments performed to evaluate the alpha phase sintering of uranium and uranium-zirconium alloys (referred as the sintering rate experiments). The experiments in Section 4.2 depended on the results in Section 4.1 because the hydride/dehydride was necessary to provide the fine uranium powder.

4.1 Powder Production Experiments

The powder production experiments are divided into three groups based on the major stages in the process development equipment described in Section 3. The following section describe the results derived using the "Airlock Setup", the "Initial Furnace Well Setups", and the Successful Furnace Well Setup."

4.1.1 Airlock Setup

Originally the powder production experimental system was placed in the west airlock. This system was used for experiments 1 through 4. The experiments were never successful do to 1) an inability to keep a constant flow of Ar-5%H_2 gas and 2) leaks in the airlock when not under pressure. Even so, small amounts of powder were produced from these experiments (Fig. 4-1), but the initial uranium slugs and the resulting powder appeared to have oxidized during the hydriding portion of the experiment.

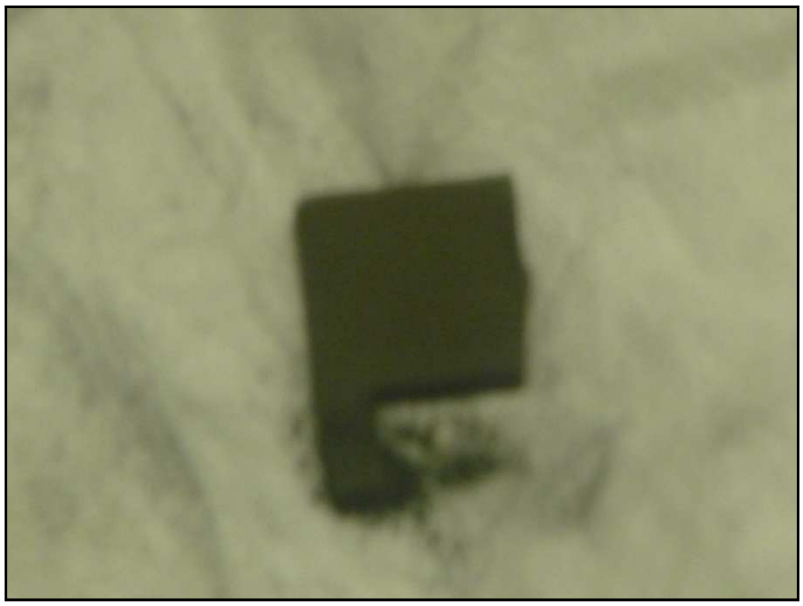

Fig. 4-1 Photo of depleted uranium piece after hydride/dehydride Experiment 3.

Experiment 1 used a depleted uranium (DU) sample with a mass of 28.0829 g. The chamber was evacuated and then filled with Argon gas. The sample was heated to a temperature of 220°C. At this point the airlock was filled with Ar-5%H_2 gas, until the pressure in the airlock reached ambient pressure (~1 atm). The sample was allowed to sit at 220°C in the Ar-5%H_2 atmosphere for 1 hour. Then the chamber was evacuated and heated to 300°C for 1 hour. The sample did not hydride or break down its structure but there was a small amount of black powder around the sample (less than 0.5 g). During the experiment the sample changed in color from silver to dark gray/black.

Experiment 2 used a DU sample with a mass of 35.5965 g. The chamber was evacuated and then filled with Ar gas. The sample was heated to 350˚C. The chamber was then evacuated and filled with Ar-5%H_2 gas. The chamber was then cycled from an Ar-5%H_2 atmosphere 3 times with the dwell time for gas atmosphere being 15, 15, and 25

minutes. The chamber was once again evacuated and brought to a temperature of 450˚C. The sample was held at this temperature for 45 minutes *in vacuo*. The results were similar to the experiment 1 results with only a small amount of black powder produced that was apparently oxidized.

Before Experiment 3 the overpressure valve was removed from the airlock to eliminate a possible source of oxygen contamination. Experiment 3 reused the DU sample from experiment 2. The mass of sample after experiment 2 and a subsequent acid washing was 34.8641g. The chamber was evacuated and then filled with Ar-5%H_2 gas. The sample was then heated to 400 ˚C and allowed to dwell in the Ar-5%H_2 atmosphere for 4.6 hours. At the end of dwell time the sample temperature was 429˚C. The sample was then allowed to cool; no attempt at hydrogen disassociation was made. There was no evidence of hydration or structural breakdown of the sample. The results were similar to the previous experiments with only a small amount of black powder produced that was apparently oxidized.

Before Experiment 4 the pressure gage was removed from the airlock to remove another possible source of oxygen contamination. Experiment 4 reused the DU sample from Experiment 1. The mass of sample post experiment 1 and a subsequent acid washing was 27.9063 g. While the chamber was flooded with Ar-5%H_2 gas, the sample was heated in vacuo to 400˚C. The sample was allowed to sit at a 400 ˚C furnace temperature in the Ar-5%H_2 atmosphere for 2.67 hours. At the end of the dwell period the sample temperature was 465 ˚C. The sample was then allowed to cool in the Ar-5%H_2 atmosphere and no attempt to dehydride was made. There was no evidence of hydration or structural break

down. The results were similar to the previous experiments with only a small amount of black powder produced that was apparently oxidized.

4.1.2 Initial Furnace Well Setups

The reaction vessel was moved into the furnace of the glovebox for the remaining experiments, beginning with Experiment 5. This section will summarize the experimental setups that were never fully successful.

In the initial design the process gas did not flow through an oxygen trap. Small amounts of uranium (~3 grams) were were inserted into the setup described in Section 3 for experiments 5 through 7. During experiment 5 the furnace was heated to 350°C under an Ar-5%H_2 atmosphere for one hour. The temperature was then lowered to 250˚C for 5 hours. No attempt to dehydride was made. After cool down the sample was a dark brown and black in color with no visible hydration or structural breakdown. When the piece was later washed in 35% volume nitric acid solution the sample turned silver, as expected, except for a dark brown line running the length of one face, Fig. 4-2. Experiments 6 and 7 were run under similar circumstances and produced similar results.

Figure 4-2 DU piece structurally intact but discolored after experiment 5

A Ti getter was added to the process gas line for experiments 9 through 12, in order to trap O_2, N_2, moisture, etc. The most successful experiment of this set was experiment 9. During experiment 9 6.2512 g of DU was placed in the reaction vessel. The Ti getter was raised to a temperature above 1000 ˚C before it was exposed to the process gas. The flow rate was kept less than 1 SCFH, and the pressure of the process was kept at approximately 5 psi (the actual pressure in the reaction vessel was most likely lower). The furnace was raised to 275˚C under an Ar-5%H_2 atmosphere and held for 15 hours. A vacuum was established periodically within the reaction vessel during the dwell time in an attempt to promote hydration of the sample. The sample was cooled and removed without attempting to fully dehydride the sample. 1.2094 grams of UH_3, a fine dark brown/black powder, was produced from the sample. The remaining sample and powder were returned to the reaction vessel.

The sample was heated to 275˚C for 24 hours and the chamber was periodically evacuated. A total of 3.1519 g of UH_3 was produced at the end of this process, Fig.4-3.

Fig. 4-3 Powder produce from experiment 9

Experiments 10 and 11 did not produce a significant amount of powder. The results were similar to experiments 5 through 8. During experiment 12 a small amount of powder, approximately 1.5 g was produce over 3 days. However, during the third day a leak in the Ti getter line was discovered. The process gas was immediately shut off and the reaction vessel was sealed off from the system. The powder produced was black in color and did not dehydride when heated under a vacuum. After experiment 12, the bottom third of the copper tubing turned yellow in color, Fig. 4-4. The yellow layer appeared to have been plated and could not be removed with a paper towel. The yellow layer remained on the reaction vessel

for the remainder of the experiments. It had no apparent effects on the experiments. After experiment 12 the Ti getter was abandoned in favor of a commercially made oxygen and moisture trap.

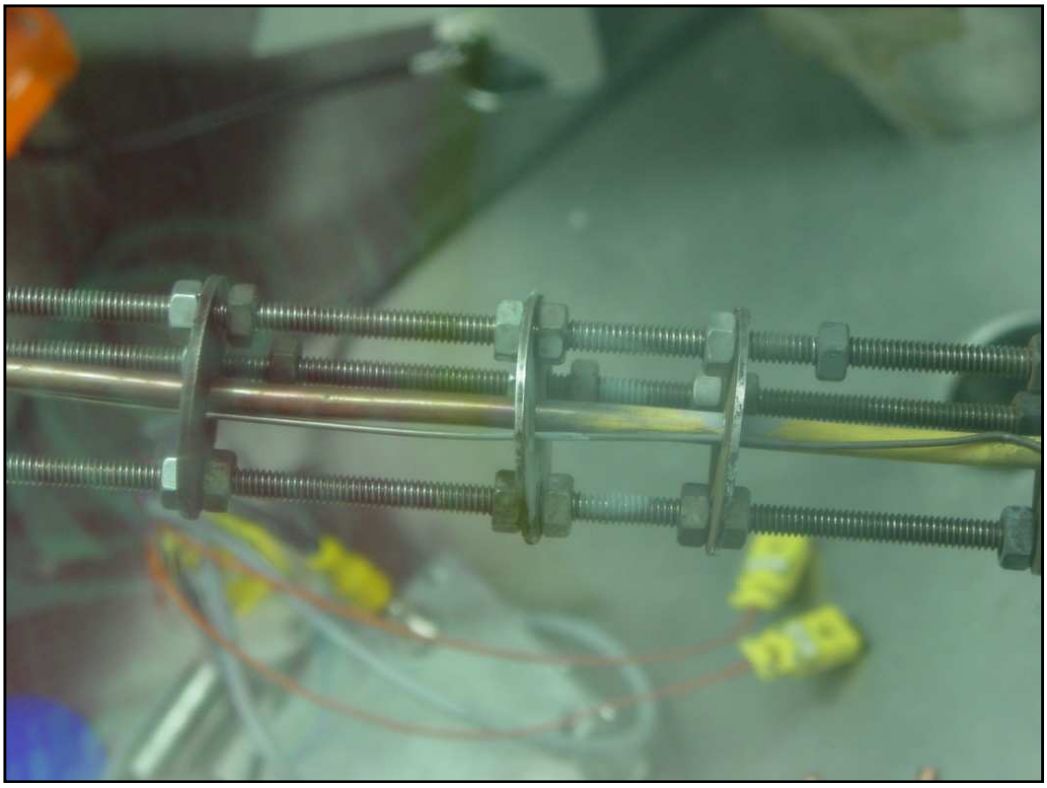

Fig. 4-4 Discoloration of copper tubing after experiment 12

4.1.3 Successful Furnace Well Setup

With the replacement of the Ti getter with the oxygen and moisture trap, Experiment 13 demonstrated a successful and repeatable hydride/dehydride process and therefore represents the final "experiment" in this section; all subsequent hydride/dehydride operations used this procedure for powder production. During experiment 13, 9.6622 grams of uranium metal powder was placed in the reaction vessel. The sample was raised to a

temperature of 265˚C for 24 hours with a flow rate of approximately 2 SCFH and the pressure of the reaction vessel was approximately 2 psi. The sample was cooled with no attempt made to dehydride. A significant amount of dark brown powder, assumed to be UH_3, was visible in the crucible. The non-hydrided portion of the DU sample along with the UH_3 powder was returned to the reaction vessel. The sample was then hydrided for an additional 24 hours under the same conditions. The sample was then place under vacuum and heated to 450 ˚C for 12 hours, this was an extreme amount of time as most literature showed a maximum time of 1 hour when dehydriding 100 grams of UH_3. The entire piece of uranium did not hydride, and the shape of the original uranium sample could be clearly seen in the sintered chunk shown in Fig. 4-5. The piece did not break under light pressure such as pressured applied by tweezers shown in Fig. 4-6, but the piece was broken apart with more applied force and weight. This is consistent with the literature of previous work.

Figure 4-5 Loose and sintered powder produce from experiment 13

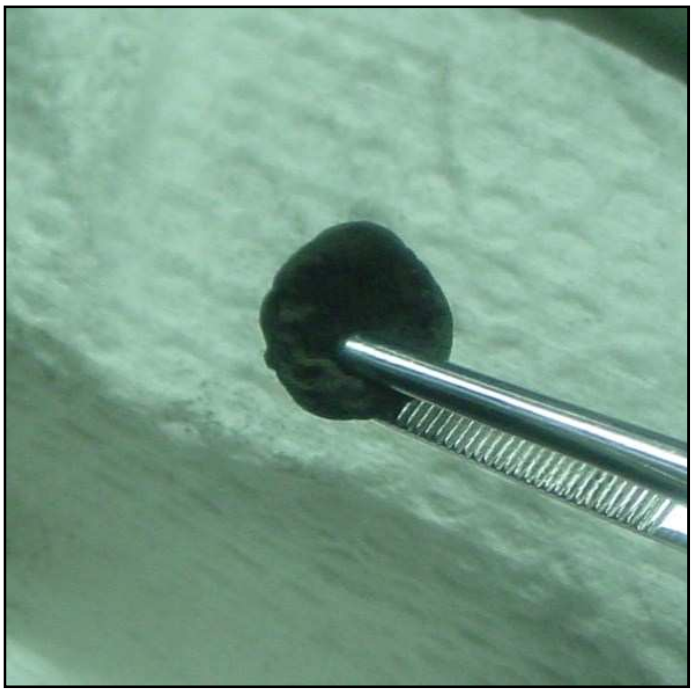

Figure 4-6 Sintered powder from experiment 13

This result was repeated throughout the rest of the experiments. The chunks were loosely sintered and could be mostly broken apart be shaking the chunk in a glass jar. The chunk was further broken apart with a stainless steel mortar and pestle. The pieces were then placed in the Wig-L-Bug and broken down with or without the addition of a stainless steel ball bearing. This process is shown in Fig. 4-7 through 4-10. The uranium, which failed to hydride, can be clearly seen in Fig. 4-11 and 4-12. The loose powder was used in a subsequent sintering experiment.

Figure 4-7 Loose and sintered powder produced post experiment

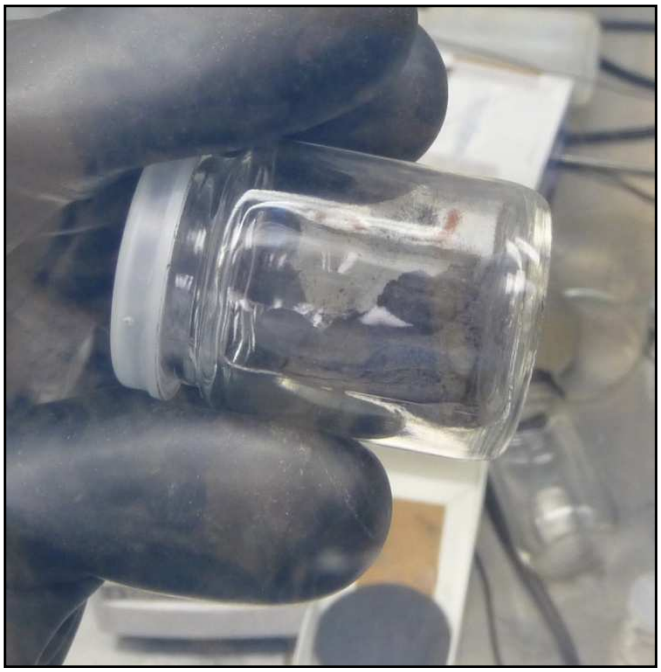

Figure 4-8 Break down of sintered powder after shaking the container

Figure 4-9 Powder, sintered chunks, and non-hydrided DU ground with mortar and pestle

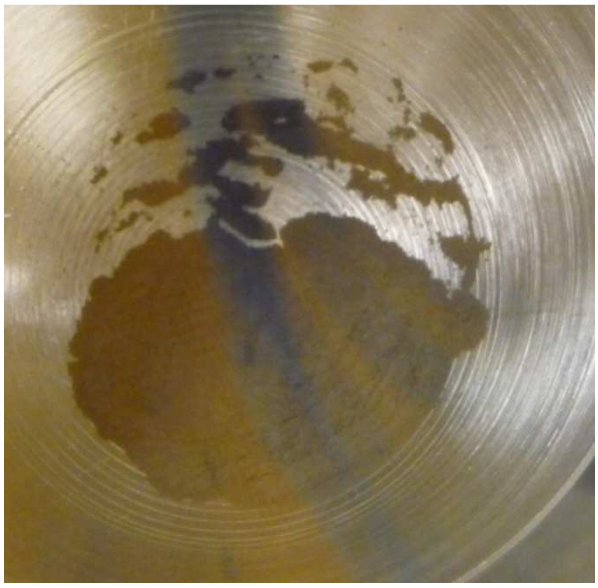

Figure 4-10 Powder after being milled in the Wig-L-Bug (sintered chunks/no hydride DU was removed)

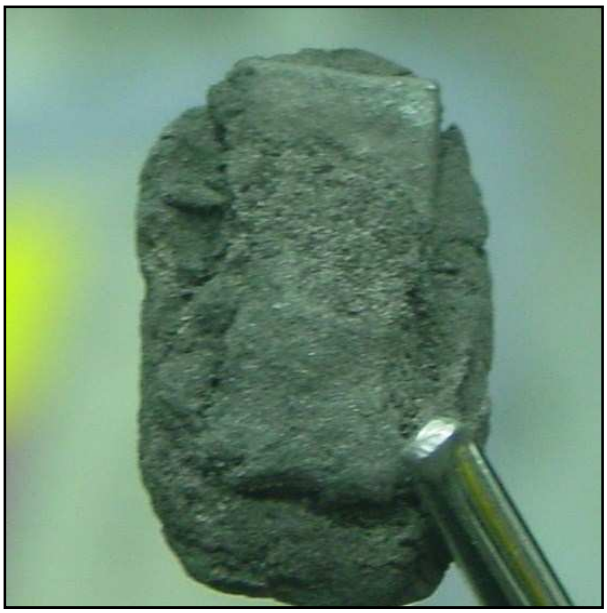

Figure 4-11 Non-hydrided DU visible and surrounded by sintered powder

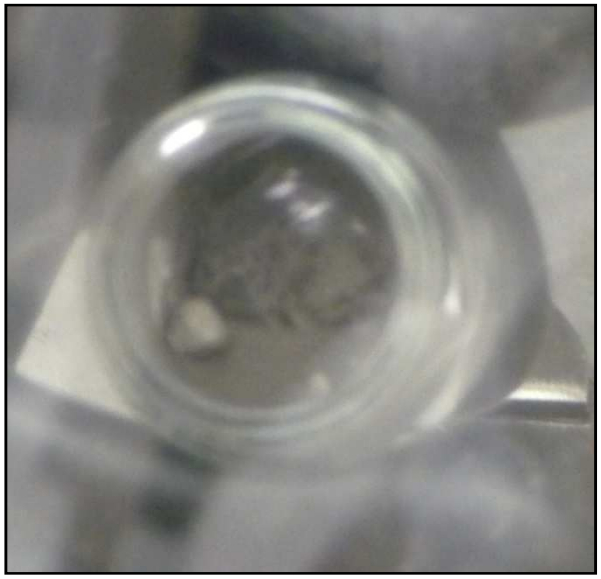

Figure 4-12 Non-hydrided DU with DU powder

The hydrogen disassociation was monitored by observing the pressure change of the reaction vessel during the dehydride phase of the experiment. The well was under a rough vacuum during dehydriding, a pressure of ~0.001 Torr. When the UH_3 would begin to disassociate the pressure on the vacuum gauge would rise. The pressure would continue to rise until a peak value was reached. At this time the pressure would stabilize and then begin to lower, as seen in Figs. 4-13 and 4-14. The dehydride was considered complete after the pressure returned to 0.001 Torr, however the sample remained at temperature *in vacuo* for an additional 15 minutes to insure full hydrogen disassociation.

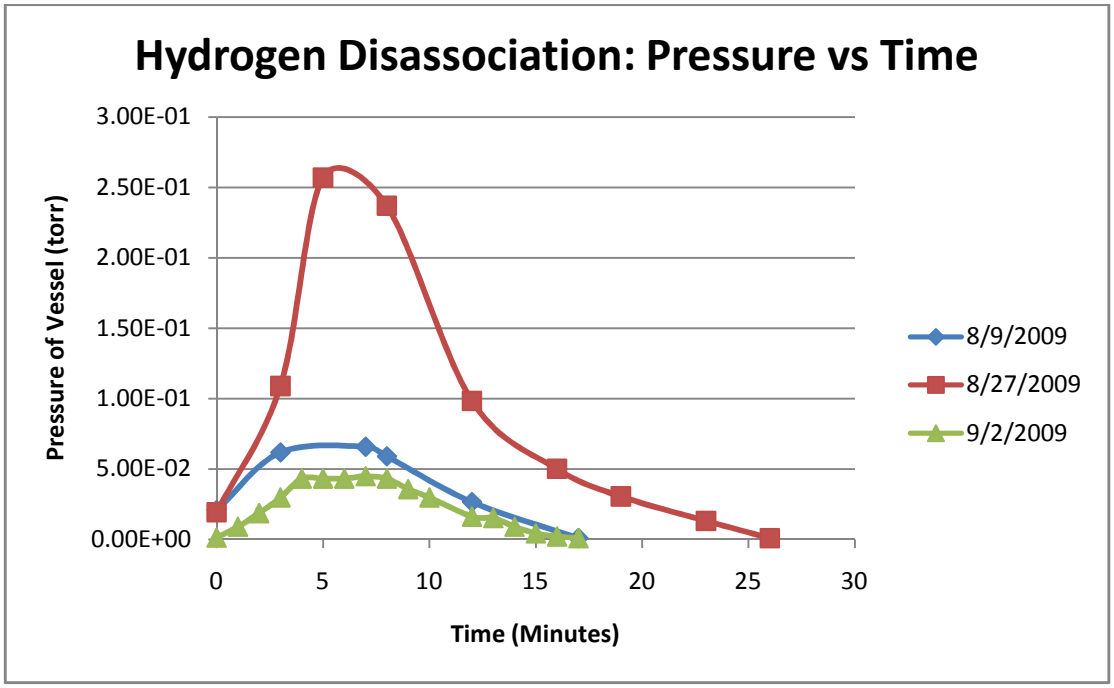

Fig. 4-13 Pressure vs Time during the dehyride step

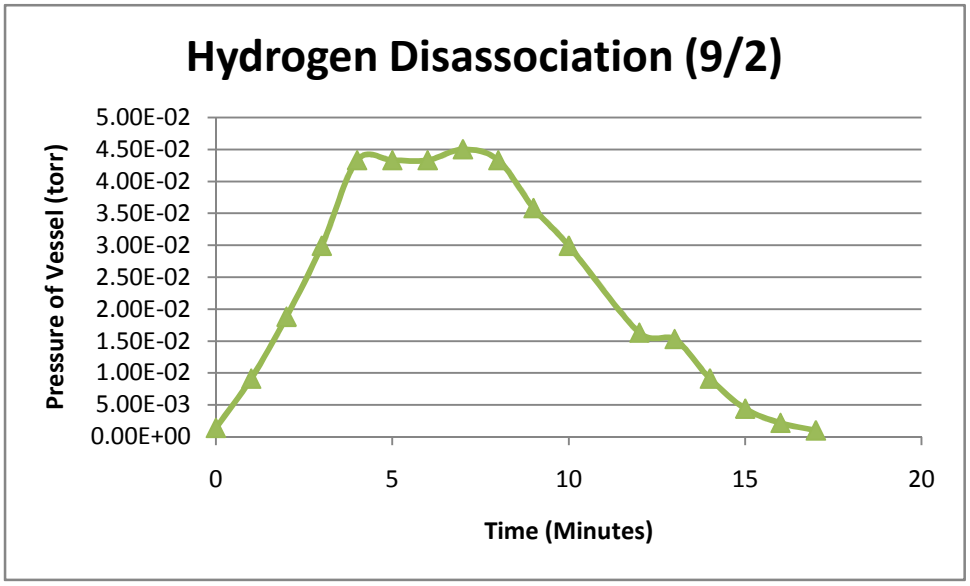

Fig. 4-14 Pressure vs Time during the dehyride step

4.1.4 Digital Microscopy of the DU Powder

A small sample of the DU powder was removed from the glovebox and examined using the KH-1300 microscope. The powder examined was produced during powder production Experiment 13. While the removed powder did oxidize, the images give a good indication of the powder size and characteristics, Fig. 4-15. The larger masses of particles are approximately 100 μm, while the smaller loose powder is on the order of 1 to 3μm. The small particles represent the majority of the powder produced by the methods described here.

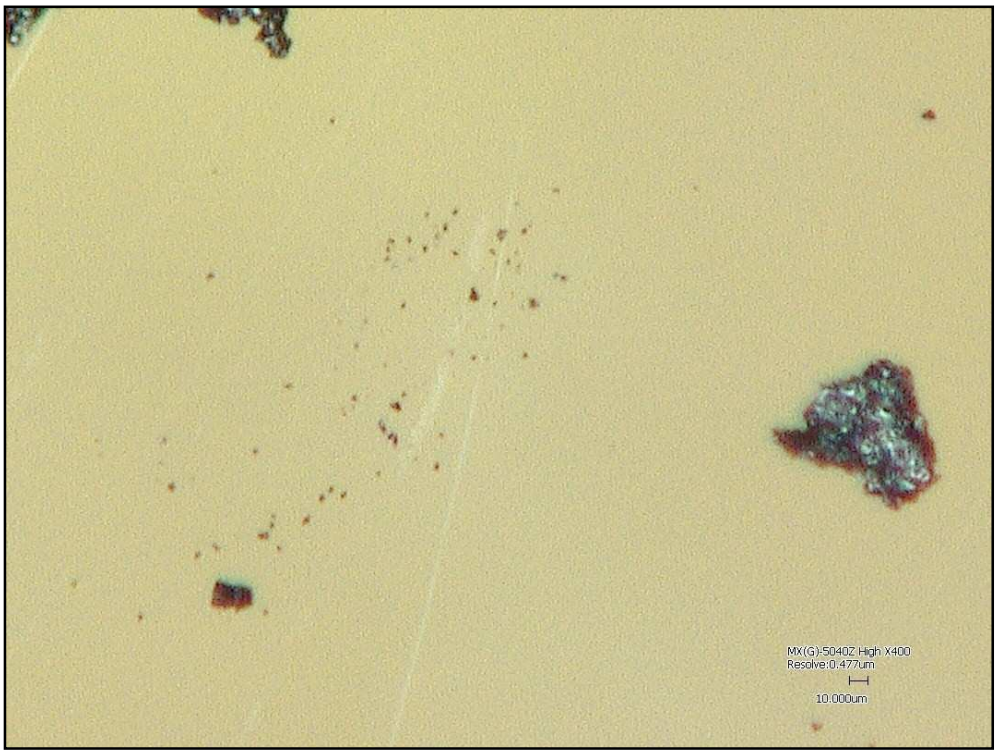

Fig. 4-15 DU at 800X

Also examined with the HIROX KH-1300 was a small piece, approx 1 mm^3, of a sintered DU chunk after the hydrogen disassociation process, Fig. 4-16 through 4-18. The sample was composed of sintered powder and was not a remnant of the original chunk. The sintered portion did not rapidly oxidize during the examination in atmosphere and did not appear to be significantly porous.

Fig. 4-16 DU powder sintered during dehydriding at 50X

Fig. 4-17DU Rough Face at 100X

Fig. 4-18 DU Smooth Face at 100X

4.2 Alpha Phase Sintering Experiments

Once the powder production method was perfected, ten pressed pellets were produced and nine were sintered for evaluation. The pellet powder compositions used in the sintering rate experiments were as follows: 5 pellets of pure DU powder, 2 pellets of DU-10Zr mixture, 1 pellet of DU-1Mg, and 1 pellet of DU-10Zr-2.4Mg (wt%). The pellet radii and heights were measured before and after sintering. In most experiments, the height change was measured during the heating using the LVDT. The samples were also analyzed using a digital microscope (HIROX KH-1300) and an SEM (JOEL-6400).

4.2.1 LVDT Calibration

The LVDT was calibrated using a horizontal motion micrometer. The LVDT magnet was moved at 0.1 in intervals from the bottom of the LVDT to the top and back again. It was determined that the rate of change was 19.1919 volts per inch, Fig 4-19. This

translates to 1.3234 mm per volt (0.0521 inches per volt). Two separate LVDTs and magnets were used during the calibration. No significant change in output was observed.

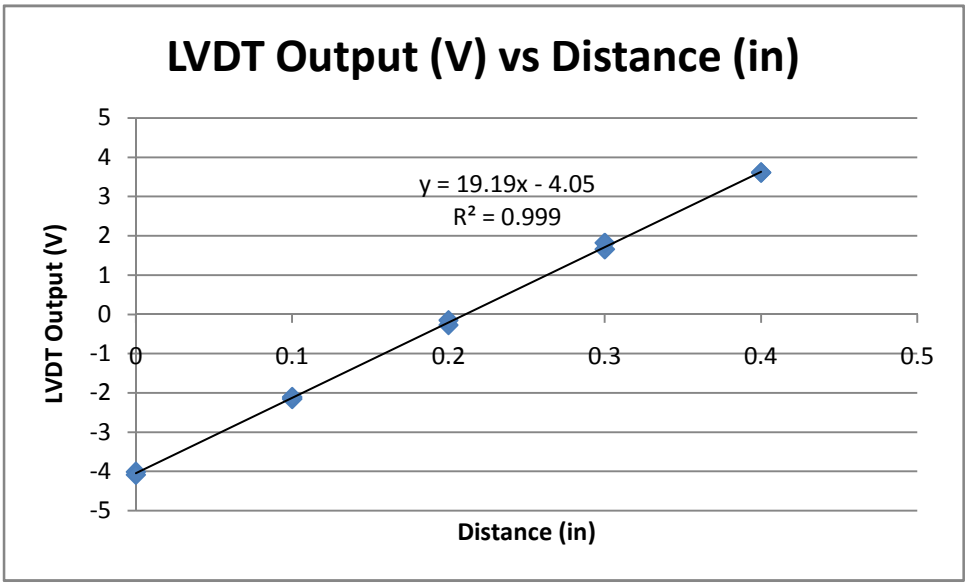

Fig. 4-19 LVDT Output vs Distance

During the sintering experiments the magnet was attached to a steel rod. The steel rod and the vessel well and the assembly hardware thermally expand during heating. In order to quantify this thermal expansion, LVDT output data was recorded without a pellet present in the sintering vessel. This was conducted for an increase from room temperature (~23˚C) to 650˚C, Fig. 4-20, and also for an increase to 700˚C and 795˚C. The data obtained from these calibration experiments were subtracted from the LVDT output obtained from the corresponding sintering experiments. This was done through the use of a data analysis code written in MatLAB.

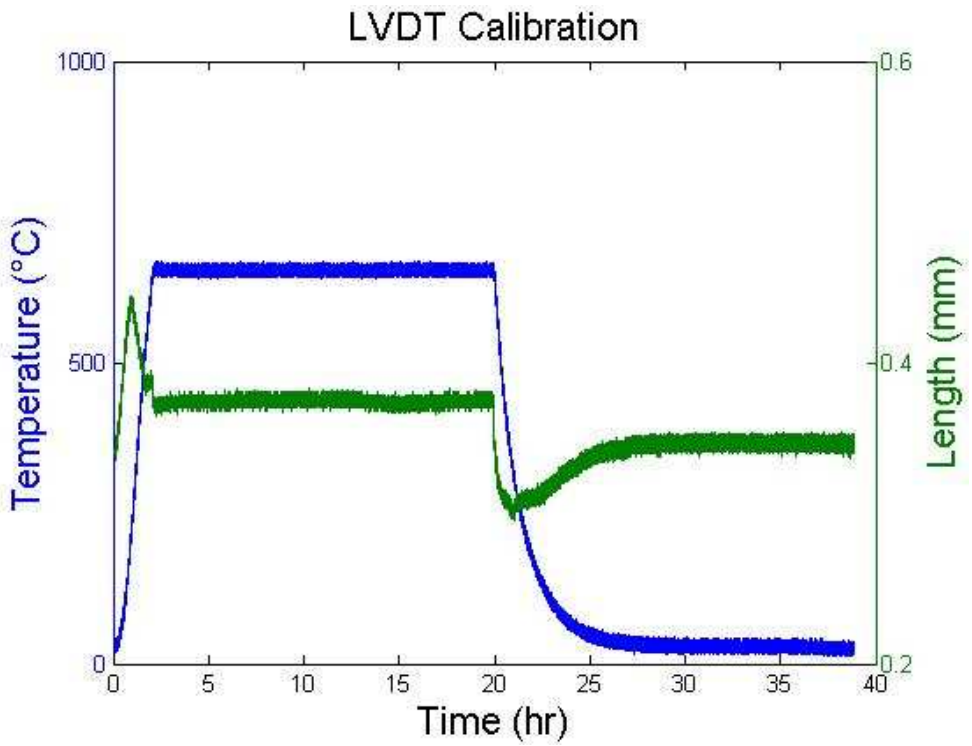

Fig. 4-20 The ramp up and ramp down of the empty system to 650 ˚C, the was an average increase of 0.3753 mm during 650 ˚C dwell time

4.2.2 Physical Observations and LVDT Data of Pellets

The pellet data for all experiments is summarized in Table 4-1 and 4-2.

Table 4-1 Pellet data pre and post experiment

Pellet #	Mass (g)	Pressed Thickness (mm)	Pressed Diameter (mm)	Green Density (% TD)	Post Thickness (mm)	Change (%)
Pellet 2	4.0368	4.3688	9.6215	66.78	4.4704	2.33
Pellet 3	3.3366	4.5288	9.6342	53.11	4.7117	4.04
Pellet 4	2.7656	2.7864	9.6622	71.13	2.8575	2.55
Pellet 5	2.9426	3.556	9.6647	63.47	3.6957	3.93
Pellet 6	2.6417	2.9667	9.6723	64.02	2.9845	0.6
Pellet 8	3.9946	5.0495	9.4234	59.6	5.2705	4.38
Pellet 9	2.9188	3.9472	9.4234	59.63	4.064	2.96
Pellet 10	2.3685	3.5712	9.6139	53.49	3.5687	-0.07

Table 4-2 Pellet data pre and post experiment (continued)

Pellet #	Post Diameter Max (mm)	Change (%)	Post Diameter Min (mm)	Change (%)	ΔL/L (from LVDT data)
Pellet 2	9.9568	3.37	9.8806	2.69	-
Pellet 3	9.8425	2.12	9.6901	0.58	0.0336
Pellet 4	9.8933	2.34	9.7409	0.81	0.0144
Pellet 5	10.1346	4.64	9.8552	1.97	-
Pellet 6	9.4488	-2.37	9.3599	-3.23	0.0506
Pellet 8	9.8171	4.01	9.3599	-0.67	0.0150, 0.0122*
Pellet 9	9.779	3.64	9.525	1.08	-
Pellet 10	9.652	0.39	9.6393	0.26	-

*ΔL/L for Pellet 8 was measured at 24 hours and 34 hours;

- indicates no LVDT was measured for that experiment

The initial pellet, pellet 1, was pressed using a double action punch and die fabricated from 303 stainless steel. The original punches were not strong enough to withstand a great amount of force, pellet 1 was pressed with a maximum force of approximately 5,000 lbs. The green density of pellet 1 was 7.75 g/cm^3 (~40.7% theoretical density). The pellet was a right cylinder with a 6.6802 mm in height and a 9.6266 mm diameter. Pellet 1 had a total mass of 3.7691 g. The pellet was placed in the furnace well and sintered for 48 hours at temperature of 640 °C. While the resulting changes in the LVDT voltage seemed to indicate sintering, the pellet broke into three large pieces inside the well (most likely on cooling). With the large piece, there was also powder in the crucible. This occurrence made any measurement of the post experiment diameter impossible. An attempt was made to measure the height of Pellet 1. While the breakage caused the accuracy of the measurements to be suspect, no shrinkage or swelling was observed.

The second pellet, as well as the rest here forward, was pressed using a 303 stainless steel die and punches fabricated from H13 tool steel which were then heat treated and tempered. This change allowed a much greater force to be applied when pressing the pellets. Pellet 2 was fabricated entirely from DU powder with a maximum pressing force greater than 15,000 lbs. This resulted in a green density of 12.69 g/cm^3 (66.6% theoretical density), Fig. 4-21. The pellet had a total mass of 4.037 g, a height of 4.3688 mm, and a diameter of 9.6266 mm Pellet 2 was sintered for 24 hours at a temperature of 650°C, 4-22. The linear displacement rod was not placed on the pellet for this experiment because it was speculated that it may have been a source of complications in the pellet #1 test. Therefore, there was no real time data of the vertical changes in the pellet. Initially, when pellet #2 was removed from the furnace no change in volume was observed; however on subsequent inspection it

was observed that the pellet had increased slightly in volume and minor cracks were evident. There was a “bump” in the center of the pellet with a maximum height measured at 4.4323 mm. The lowest height measured was 4.3688 mm. The diameter of the pellet was mostly uniform except on one end where it bowed out. The diameter of the non-bowed portion of the pellet was 9.8171 mm. The end portion of the pellet had a measured diameter of 9.9060 mm.

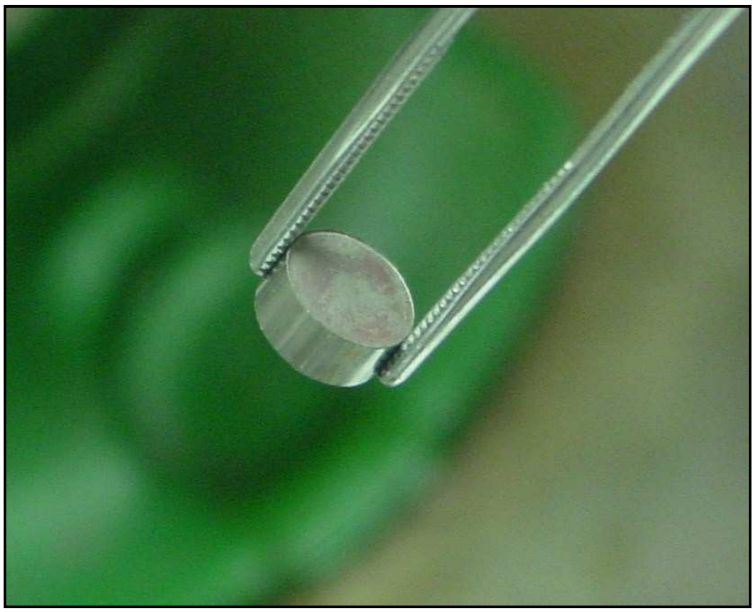

Fig. 4-21 Pellet 2 pre sinter

Fig. 4-22 Pellet 2 post sinter

Pellet 3 was pressed with a maximum load of 15,000 lbs. The green density of this pellet was 10.16 g/cm^3 (53.3% T.D.). Pellet #3 had a total mass of 3.3365 g, a height of 4.5085 mm, and diameter of 9.6266 mm. The pellet was heated to 650˚C for 24 hours, Fig. 4-23. The vertical change in the pellet during the experiment is shown in Figs. 4-24 and 4-25. It is interesting to note that the LVDT data indicates sample shrinkage and the post-test measurements indicate sample growth. Upon completion of the experiment, the final height was measured to be 4.7879 mm, an increase of 6.20%. Also the diameter of the pellet was tapered. A measurement was taken at both ends and in the middle of the pellet. The ends had a diameter of 9.4996 mm and 9.7536 mm. The middle of the pellet was measured at 9.6266 mm, a zero net change in size.

Fig. 4-23 Pellet 3 post sinter rate experiment

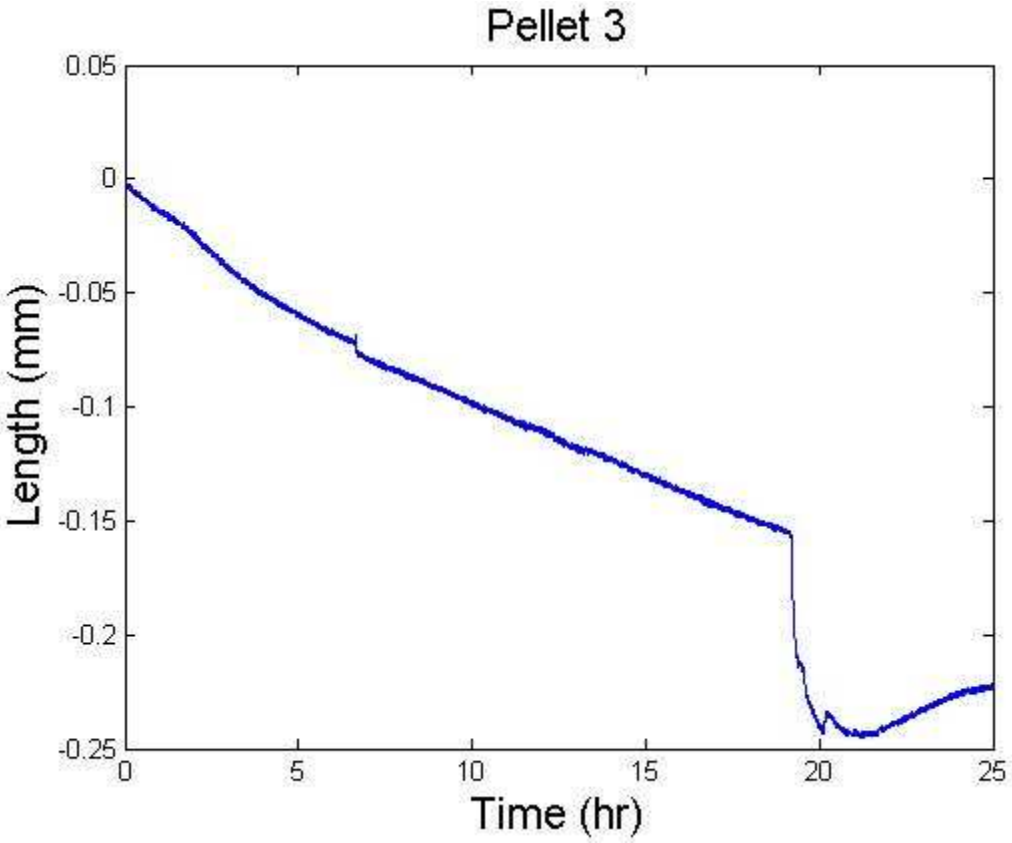

Fig. 4-24 The linear shrinkage of the Pellet 3, with time 0 beginning when the system reached an equilibrium at 650°C

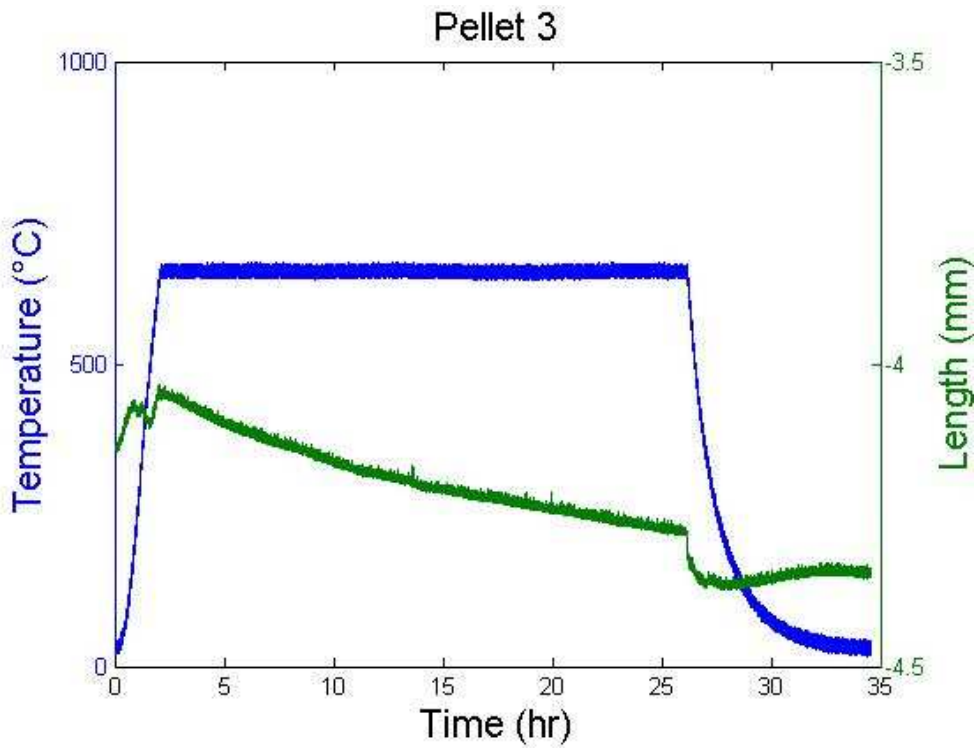

Fig. 4-25 Uncalibrated pellet 3 shrinkage data with temperature

Pellet 4 was press with a maximum load of 15,000 lbs. The initial height and diameter were 2.7864 mm and 9.6622 mm, respectively. The mass of the pellet was 2.2677 g, giving the pellet a green density of 71.3% theoretical density (11.19 g/cm$^{3)}$. The pellet was heated to 655˚C and allowed to dwell at this temperature for 30 minutes. Then the pellet was raised to 695°C, the beta phase, and allowed to dwell for 30 minutes before being cooled back to 655°C. This process was repeated once more, and then the pellet was allowed to dwell at 655°C for 5 hours. Post experiment, the pellet expanded both vertically and linearly. There was a gradient to the radial expansion of the pellet; the small expanded to 9.7409 mm, while the large end expanded to 9.8933 mm. The pellet expanded vertically to 2.8677 mm, however the LVDT data showed a continual decrease in length (see Figs. 4-

26 and 4-27). The phase transitions were too short in duration to be able to discern usable data from the system response to the temperature increase.

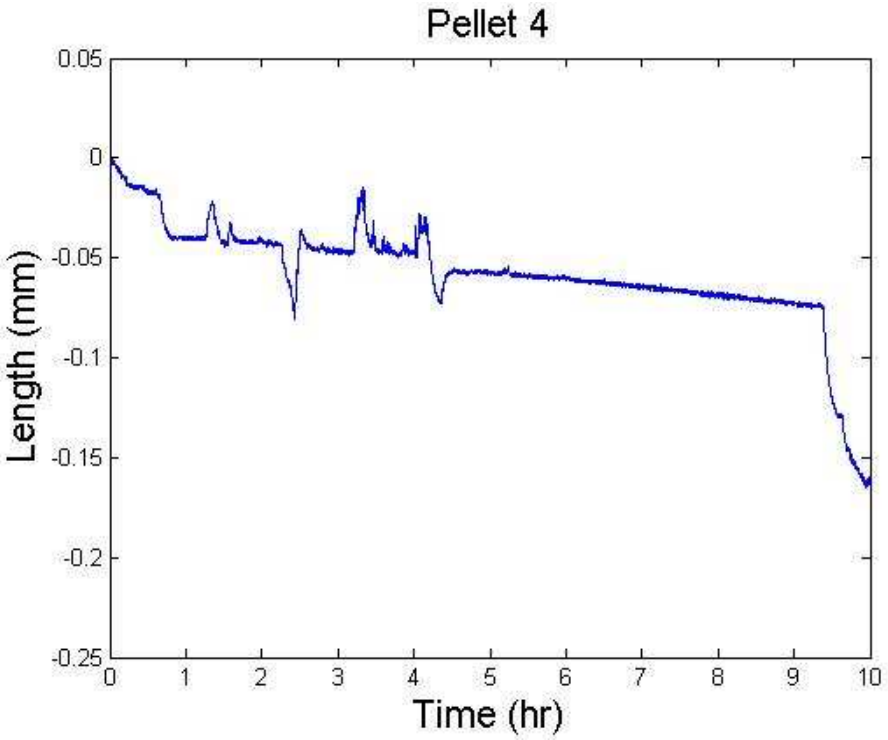

Fig. 4-26 The linear shrinkage of the Pellet 4, with time 0 beginning when the system reached an equilibrium at 650°C

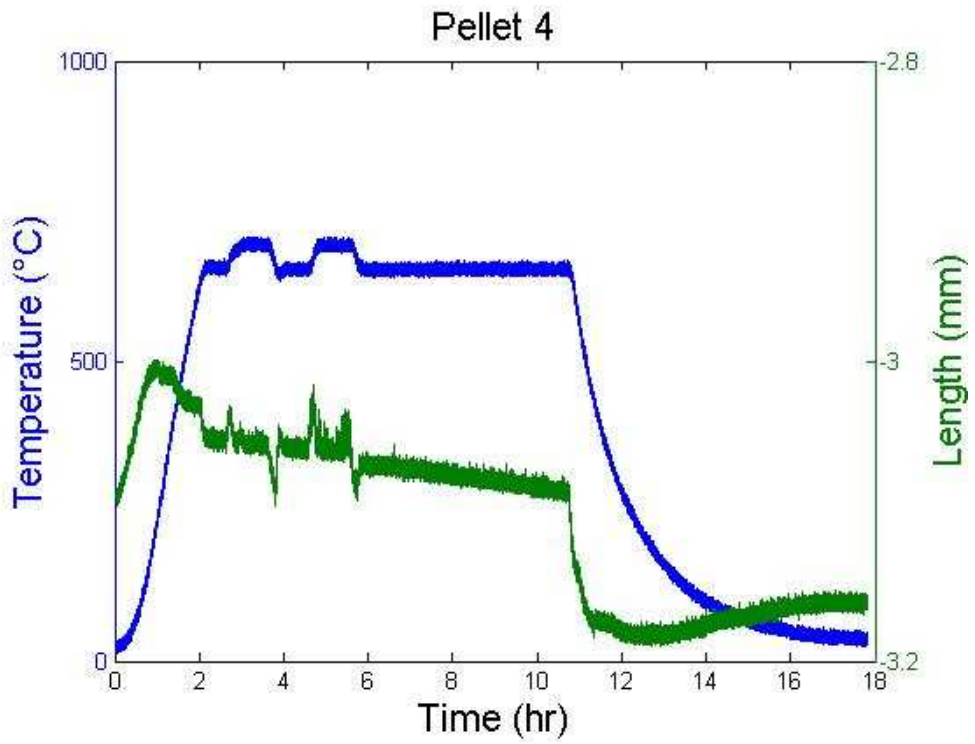

Fig. 4-27 Uncalibrated pellet 4 shrinkage data with temperature

Pellet 5 was fabricated as a DU-10Zr (Wt %) pellet. The masses of the powder used for this pellet were 2.7365 g of DU and 0.3055 g of Zr (the Zr powder was -325 mesh). The powder was placed in the Wig-L-Bug and mixed until homogenous. The final weight of the pressed pellet was 2.9438 g, a loss of 0.0982 g (3.2%) of material. The height and diameter of the pressed pellet was 3.5560 mm and 9.6673 mm respectively, which gives the pellet a green density of 63.47% theoretical (11.27 g/cm$^{3)}$. The pellet was held at 650°C for 12 hours, and then it was cycled three times from 650°C to 700°C with each cycle lasting between two and three hours. After the experiment, there was a visible second phase on the outside of the pellet (Fig. 4-28). The sintered pellet was conical in shape with one end having a diameter of 10.1219 mm and the other having a diameter of 9.8552 mm. The

thickness of the pellet was also slightly uneven with the shortest measurement being 3.6957 mm and the longest being 3.7592 mm. The LVDT data for the pellet is shown in Figs. 4-29 and 4-30.

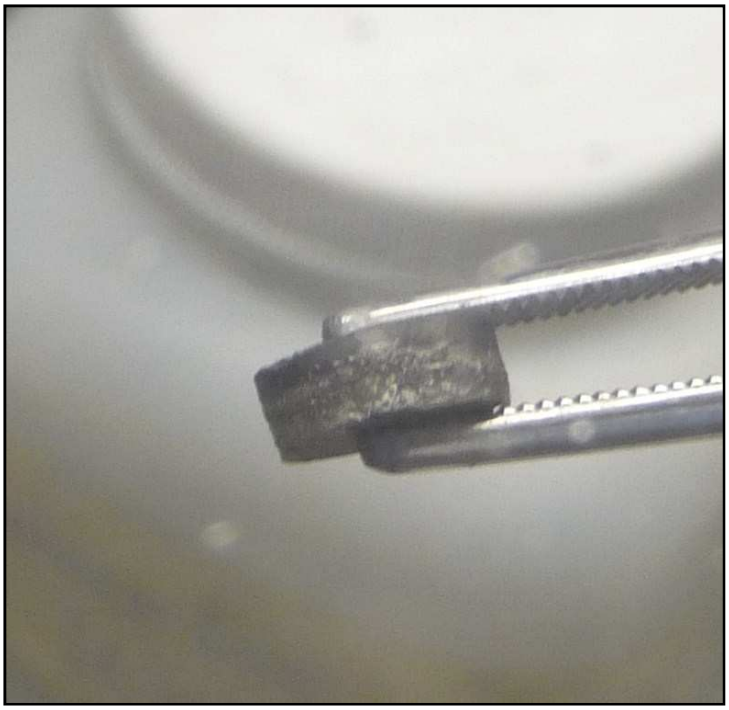

Fig. 4-28 Pellet 5 post experiment

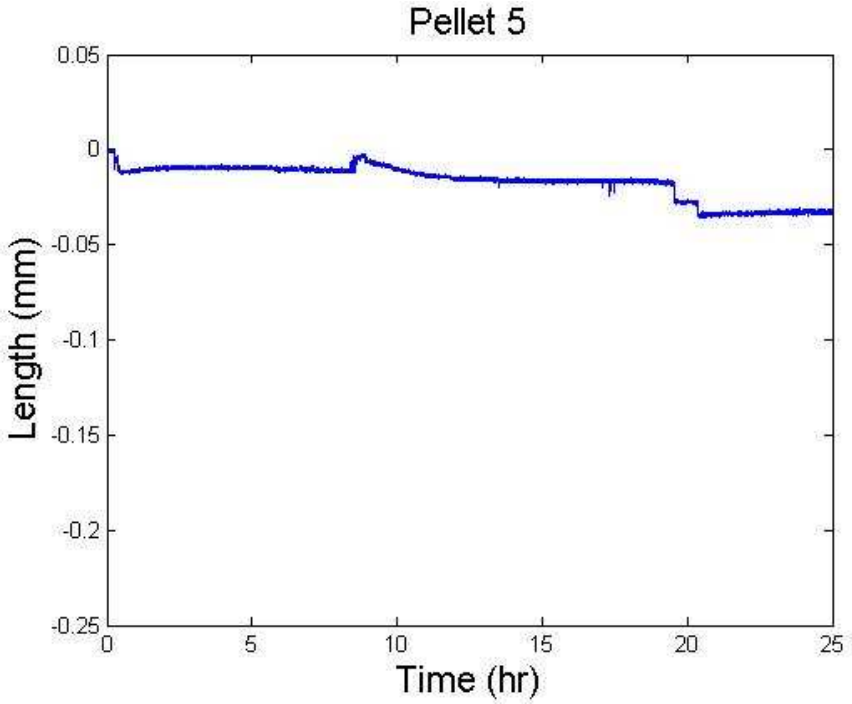

Fig. 4-29 The linear shrinkage of the Pellet 5, with time 0 beginning when the system reached an equilibrium at 650°C

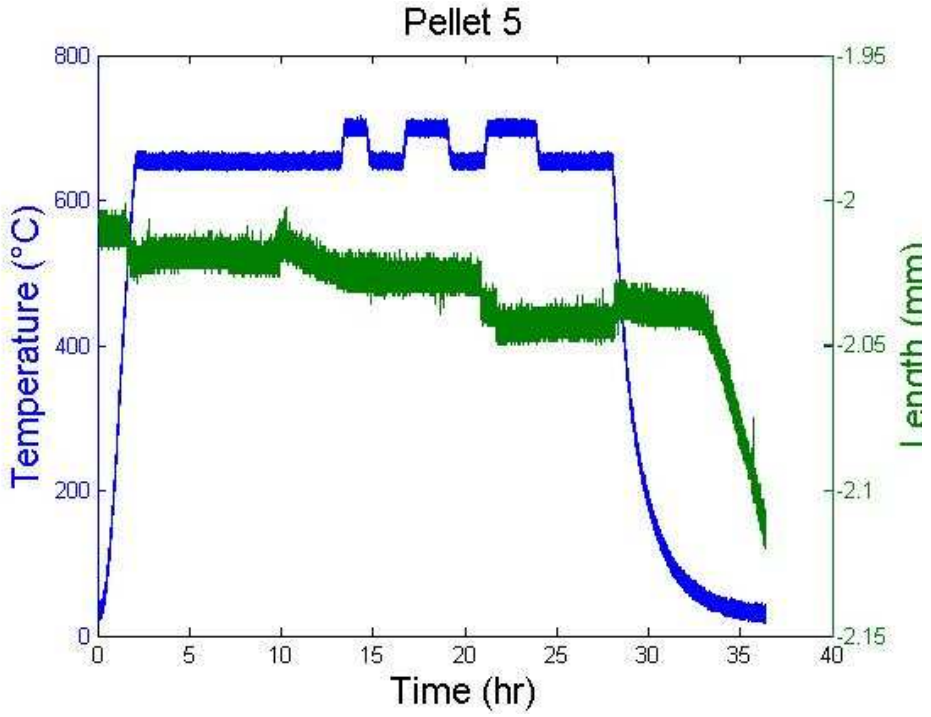

Fig. 4-30 Uncalibrated pellet 5 shrinkage data with temperature

Pellet 6 was a DU-Mg pellet. Mg was used as a surrogate for Pu in order to simulate the liquid phase sintering that would occur in a DU-Zr-Pu pellet. Mg was chosen because it has a similar melting point to Pu (640°C for Pu vs. 650°C for Mg). Because Pu has a much higher density than Mg, it was not prudent to use the same weight percent of Mg in the pellet to simulate plutonium. Instead, the atom % of Pu in a DU-10 wt. % Pu was calculated such that the Mg addition would be analogous to the Pu atom percent A 3 gram U-10 wt% Pu alloy pellet contains 0.00123 moles (0.3 g) of Pu. 0.00123 moles of Mg has a mass of 0.0290 g. Thus the pellet composition was DU-1Mg (wt%).

Pellet 6 was pressed using 2.7058 g of DU and 0.0290 g of Mg. The weight of the pellet after pressing was 2.641 g. The pressed dimensions of the pellet were a thickness of 2.9667 mm and a diameter of 9.6723 mm. This gave the pellet a green density of 64.02%

theoretical density, (12.11 g/cm$^{3)}$. The post experimental thickness of the pellet was 2.9845 mm. The pellet was conical shaped with one end having a diameter of 9.4488 mm and the other having a diameter of 9.3599 mm. During the sintering experiment there was a malfunction with LabView program which halted the data collection; therefore there is no real time sintering data was available.

Pellet 7 was a DU pellet that was pressed with a max load of 15,000 lbs. The pellet was not sintered and was fabricated to use as a structural comparison to the sintered pellets. Pellet 7 went through rapid oxidation while being prepared for analysis outside of the glovebox. Due to this event no useful data about the pellet structure could be obtained.

Pellet 8 was DU pellet that was press with a maximum load of 12,000 lbs. The pressed dimensions of the pellet were a thickness of 5.0495 mm and a diameter of 9.4234 mm. This gave Pellet 8 a green density of 59.60% theoretical density. The pellet was held 650°C for approximately 12 hours, then it was raised to 700°C for approximately 6 hours, then raised again to 796°C for approximately 4 hours, and finally the temperature was lowered back to 650°C for 6 hours. These temperature variations were used in order to observe changes in the linear shrinkage over the three phases, Figs. 4-31 and 4-32. Post experiment the thickness of the pellet was 5.2603 mm. The pellet was conical shaped with one end having a diameter of 9.3599 mm and the other having a diameter of 9.8171 mm, Fig. 4-33.

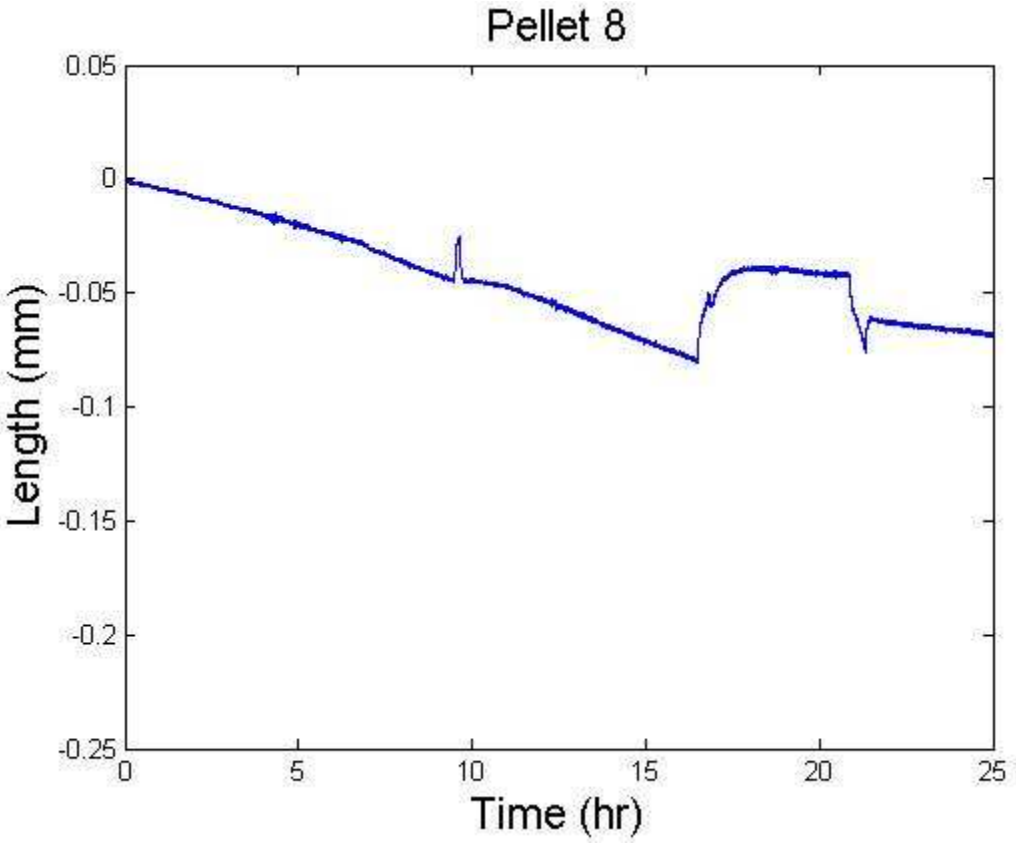

Fig. 4-31 The linear shrinkage of the Pellet 8, with time 0 beginning when the system reached an equilibrium at 650°C

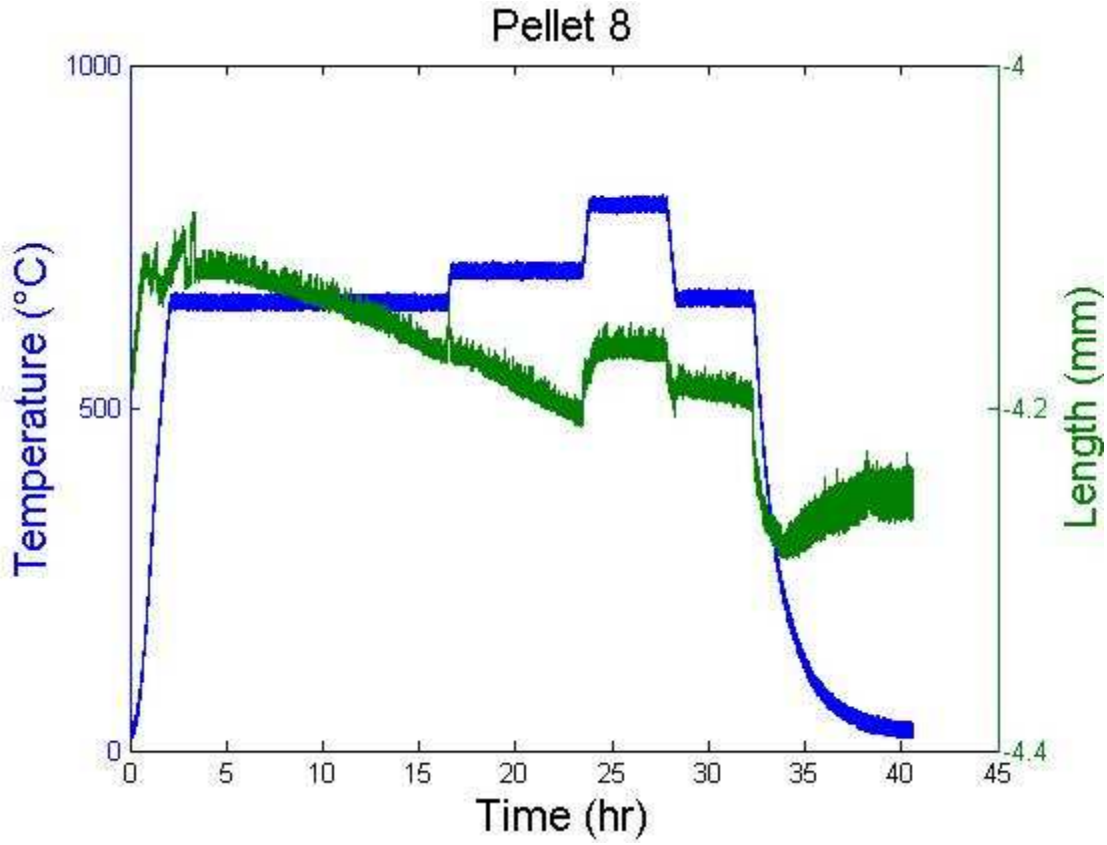

Fig. 4-32 Uncalibrated pellet 8 shrinkage data and temperature

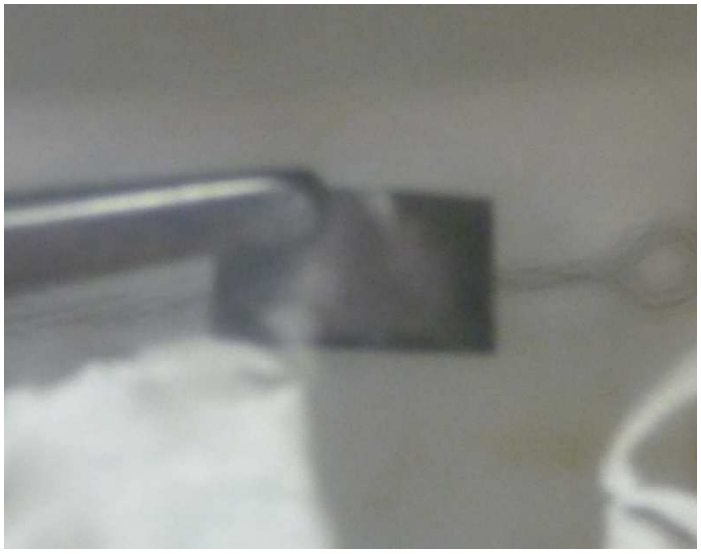

Fig. 4-33 Pellet 8 post experiment, pellet 8 is conical shaped

Pellet 9 was fabricated as a DU-10Zr pellet. The pellet was pressed with a maximum load of 14,000 lbs. The powder was fabricated from 2.6996 g of DU and 0.3004 g of Zr powder, Fig. 4-34. The final weight of the pressed pellet was 2.9188 g. The pressed thickness of the pellet was 3.9472 mm and the diameter was 9.4234 mm. This gave the pressed pellet a green density of 59.63% theoretical density (10.60 g/cm$^{3)}$. The pellet was heated to 650°C and held for approximately 12 hours. It was then raised to 695°C and held for approximately 4 hours. The pellet was then raised to 770°C and held for approximately 4 hours. When pellet 9 was removed from the reaction vessel, it was observed the bottom had been broken (Figs. 4-35 and 4-36). The bottom was rough and powder was continually falling off of the pellet at this point. As the pellet was being measured, the outside of the pellet began to breakaway. This made obtaining an accurate post experiment diameter or thickness impossible. The thickness measured was 4.0563 mm and the diameter was between 9.7790 mm and 9.5250 mm. During this experiment, there was a malfunction with the LVDT system which caused extreme swings in voltage thus making most the obtained data useless. However the initial data, at 650°C, did not suffer from these voltage swings. The data obtained was analogous to pellet 5, also a DU-10Zr pellet.

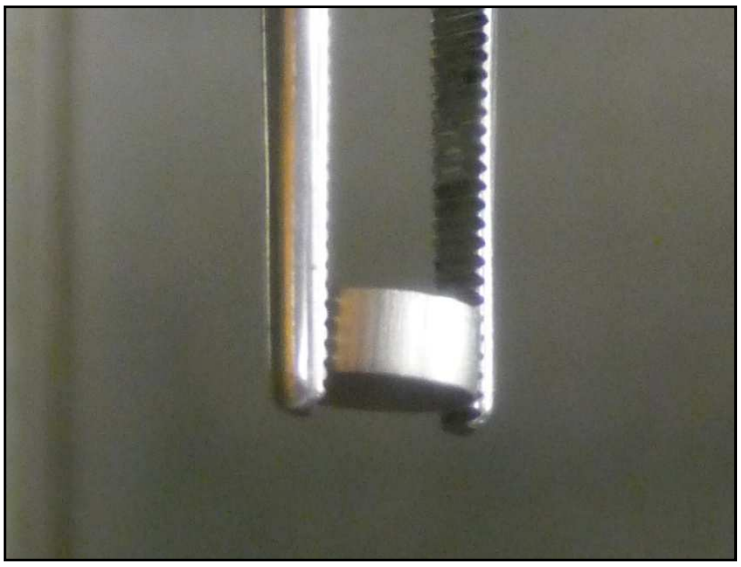

Fig. 4-34 Pellet 9 (DU-10Zr Wt %) pre experiment

Fig. 4-35 Pellet 9 (DU-10Zr Wt %) post experiment

Fig. 4-36 Pellet 9 (DU-10Zr Wt %) post experiment

Pellet 10 was fabricated as a DU-10Zr-2.4Mg pellet. The amount of Mg used was an equivalent At % as the amount of Pu in a 3g DU-10Zr-20Pu pellet. A 3 gram U-10Zr-20 wt% Pu alloy pellet contains 0.00246 moles (0.6 g) of Pu. 0.00246 moles of Mg has a mass of 0.0597 g. The mass of the components used to fabricate pellet 10 are as follows: DU 2.0998 g; Zr 0.3009; Mg 0.0595 g. The final mass of the pressed pellet was 2.3685 g. The powders were mixed together using the Wig-L-Bug until homogenous. The pressed thickness of the pellet was 3.5721 mm and the diameter was 9.6139 mm. This gave pellet 10 a green density of 53.49% theoretical density (9.13 g/cm$^{3)}$. The pellet was heated to 655°C and allowed to dwell at this temperature for 12 hours. Post experiment there was very little change in the dimensions of the pellet. The diameter was measured to be 9.6418 mm and the thickness was measured to be 3.5662 mm. The pellet was golden in color and

there was a dark mark on one side (Figs. 4-38 and 4-39). The portion with the dark mark was not as structurally stable as the rest of the pellet and was fragile when probed.

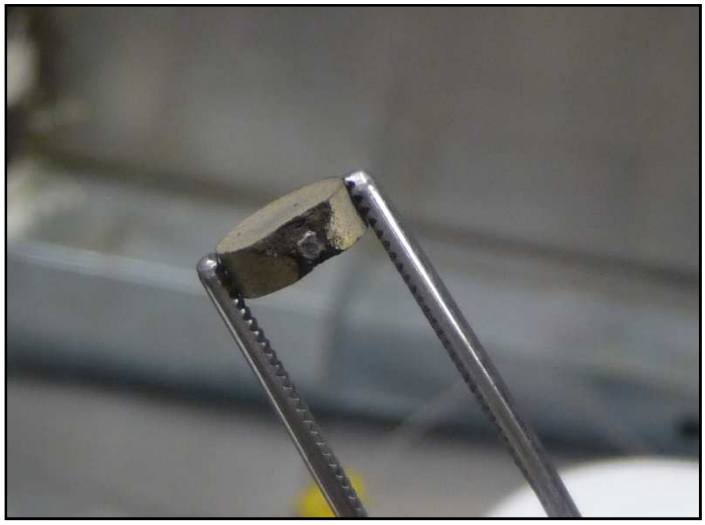

Fig. 4-37 Pellet 10 post experiment, pellet was gold and structurally damaged

Fig. 4-38 Pellet 10 post experiment, pellet was gold and structurally damaged33

4.2.3 Microscopy of the Pellets

The HIROX KH-1300 digital microscope and JOEL-6400 SEM were used to examine the pellets after sintering. The images were analyzed to characterize the the structure, porosity, and phase compositions. All pellets showed varying degrees of sintering and porosity. One constant was the presence of various sized cracks; the largest cracks were not captured during SEM imaging (in other words, the images were taken from regions between large cracks). The cracks appeared in greater frequency along the edges of the pellet. Porosity estimates were only able to be calculated for Pellets 2, 3, and 6, due to limitations of the SEM JOEL-6400. The pores in the SEM images of pellet 5 and 10 were obscured to the point at which an accurate porosity measure was not viable. The porosity was calculated using the image analysis software Image J. Using this software a number of pixels making up the pores were counted and the ratio of these pixels to the total pixels of the image was calculated. A detailed analysis of these images can be found in Section 5.2.2.

5. DISCUSSION OF RESULTS

5.1 Powder Production

5.1.1 Successful Development of a Powder Production System

A system to produce fine DU powder via the hydride/dehydride method was successfully designed and developed, but there were a number of key design changes along the way that highlight the need for gas purity, metal surface preparation, and well controlled vacuum conditions. In the final method, uranium slugs were hydrided at 225˚C to form UH_3 powder and dehydrided at 375˚C to form U metal powder. After the hydrogen disassociation step the powder was loosely sintered into fragile agglomerates. The agglomerates were broken apart using a stainless steel mortar and pestle and mechanical milling. These results agree with previous literature (Chiotti, Wilkinson). Using various starting DU masses (approximately 10-20 g), a single powder production run produces 6 to 12 g of fine DU powder in approximately 48 hours. The particle size of powder produced was on the order of 1 to 3 μm after mechanical milling. This system can be scaled up to produce a greater amount of powder.

5.1.2 Initial Failures and Contamination

The initial failures of the powder production experiment were indicative of contamination, most likely oxygen, in the process gas or hydriding environment. The contamination can cause a competing reaction with the hydrogen, in this case oxidation. This can inhibit or completely overtake the hydrogen reaction with the uranium. Even if hydriding and dehydring is successful in producing powder, oxygen contamination will also result in oxidation of the uranium powder. This was evident in the powder produced during

experiment 9 and the inability to dehydride to a pure DU powder. The leak that occurred during experiment 12 was obviously a major source of contamination, as well. This contamination led to the oxidation of the sample and all powder produced and also caused a "yellow" deposit to plate on the copper tubing in the reaction vessel. In an effort to rid the device of this deposit or at least limit its reactivity with any later experimental samples, the vessel was placed under an Ar-5%H_2 flow, heated to 500˚C for a short time and then the vessel was evacuated. The deposit appeared unchanged and showed no indication of reacting with the hydrogen flow. While the deposit was not effectively removed, it did not interact with process gas at operating temperature and therefore was not a concern of contamination during the subsequent experiments. The deposit remained on the reaction vessel hardware for the remainder of the powder production experiments with no visible impact on the sample or powder.

5.1.3 Powder Production Limitations

There were several factors which limited the production of UH_3 in the early development experiments. These factors include the ambient pressure of the hydrogen gas over the sample, temperature of sample, the percentage of hydrogen in the process gas, the surface area of the sample, and the previous mentioned oxygen contamination. In order maximize the effectiveness of the powder production the temperature and pressure parameters were adjusted throughout the experiments. The final settings had the pressure in the reaction vessel set to 2 psi, or 0.136 atm, over atmospheric pressure. This pressure was chosen due to its favorable hydrogen pressure, above atmosphere, for the UH_3 reaction. Due to the limitations of the powder production experimental set-up (glass overflow trap,

rubber stopper with weights, etc.), 2 psi was as high as the pressure of the reaction vessel could be safely raised without causing new complications.

The ideal temperature of the sample during hydration was found to be 235˚C, this is 10˚C above the consensus ideal hydration temperature. The temperature of the sample was increased because of the cooling effect the process gas had on the sample. Another factor which severely limited the rate and the quantity of DU powder producion was the composition of the process gas. The composition used throughout the experiments was Ar-5%H; this was chosen for safety reasons as H_2 is extremely flammable. The limited amount of H_2 in the reaction vessel, which limited the interaction between the hydrogen and DU sample. In an attempt to offset this limitation and increase the chances of a H_2 DU interaction, the process gas flowed directly over top of the sample at the relatively slow rate of approximately 2 SCFH. Another limitation of the powder production was the exposed surface area of the DU samples. This limitation was caused mainly by the size of the furnace well which directly led to the size of the reaction vessel. The samples were placed into a 10 mL cylindrical crucible. As the sample would hydride the bottom of the crucible would fill with powder, effectively limiting the ability of the process gas to reach the bottom portions of the sample until the original DU piece was surround of UH_3. This is evident by the non-hydrided portions of the samples being incased in the sintered DU powder post experiment.

5.1.4 Limitations on DU Powder Characterization

The powder production experiments successfully produced DU powder from experiment 13 onward; however the characterization of the powder was met with several limitations. From the physical observations the, process seemed to cause total or near total disassociation of the hydrogen from the DU. The powder was a dark gray in color, not black or dark brown. The powder sintered into loosely formed aggregates during the dehydriding phase of the process, and the resulting powder was very fine 1-3 microns. Due to the pyrophoric and radioactive nature of the material, characterization of the powder beyond physical observation proved to be difficult. A small sample of the power, < 0.1 mg, was placed in a Petri dish, removed from the glovebox and examined with KH-1300. The powder oxidized upon contact with air such that some of parts of the plastic Petri dish melted from the heat. Still the examination was successful in characterizing the size of the DU powder, albeit that the powder anylyzed was heavily oxidized.

It would be valuable to have the element composition characterized. This information would help determine if there are any contaminates in the powder, such as oxygen, or if the powder had fully dehydrided. Oxygen is a strong hindrance to the sintering of metal powders. UH_3 could also have notable effects on the sintering of DU pellets. Unfortunately no facility could be found on campus that was willing to characterize the powder due to the nature of DU. Characterization was performed on the sintered pellets using the EDS ability of the JOEL-6400; no significant contaminants were found in the pellets.

5.2 Alpha Phase Sintering Experiments

5.2.1 Proof of Concept of Alpha Phase Sintering and the System Design

SEM analysis showed various degrees of sintering in all the pellets examined. The pellets all showed visible signs of sintering via necking between particles grain growth, and pore morphology. The amount of sintering was not consistent throughout the pellets. There were areas with very low porosity and areas where no sintering appeared to occur (the initial powder particles were clearly visible). Despite these inconsistencies in porosity/sintering, the alpha phase sintering experiments were considered to successfully demonstrate that alpha phase sintering was achieved and that a reliable means of quantifying the sintering process has been established.. These experiments show that densification of powdered pressed DU/DU-Zr pellets will happen at temperatures below 660 ˚C. The lowest porosity samples contained Mg which caused liquid enhanced sintering to occur in the pellets; a similar phenomenon will occur if Pu metal is incorporated into this type of fuel form.. Using these experiments as a basis, a test matrix can be developed to calculate the activation energy of alpha sintering and the sintering rate for various pellet compositions.

5.2.2 SEM Image Analysis

The SEM image analysis performed provided the most robust evidence of sintering in the pellets. There are visible signs of sintering in all of the images. The pellets also are all consistently more porous near the radial edge. The reason for this is not clear, but uneven expansion/contraction during cool down maybe a contributing factor. Conglomeration of the powder is believed to be another contributing factor to the inconsistencies in porosity. This conglomeration is characteristic of a non-uniform powder particle size. The non-uniform powder particle size was most likely caused by insufficient milling of the powder.

As noted in Table 4.1, Pellet 2 was 100% DU sintered at 650°C, and it was found to have a porosity of 18 ± 3% using the pixel counting method in the Image J software.

Evidence of sintering can be seen in Fig. 5-1. Most of the original particles (1-3 μm) have sintered into large grains and are completely indistinguishable. In the areas of lower sintering there are visible signs of necking between separate powder particles. There are also areas of the pellet where very little sintering has taken place and the individual particles are intact. The various degrees of sintering can be attributed to variation in density in the green pressed pellet and conglomeration of particles, Section 5.2.3 contains a more detailed analysis of this phenomenon.

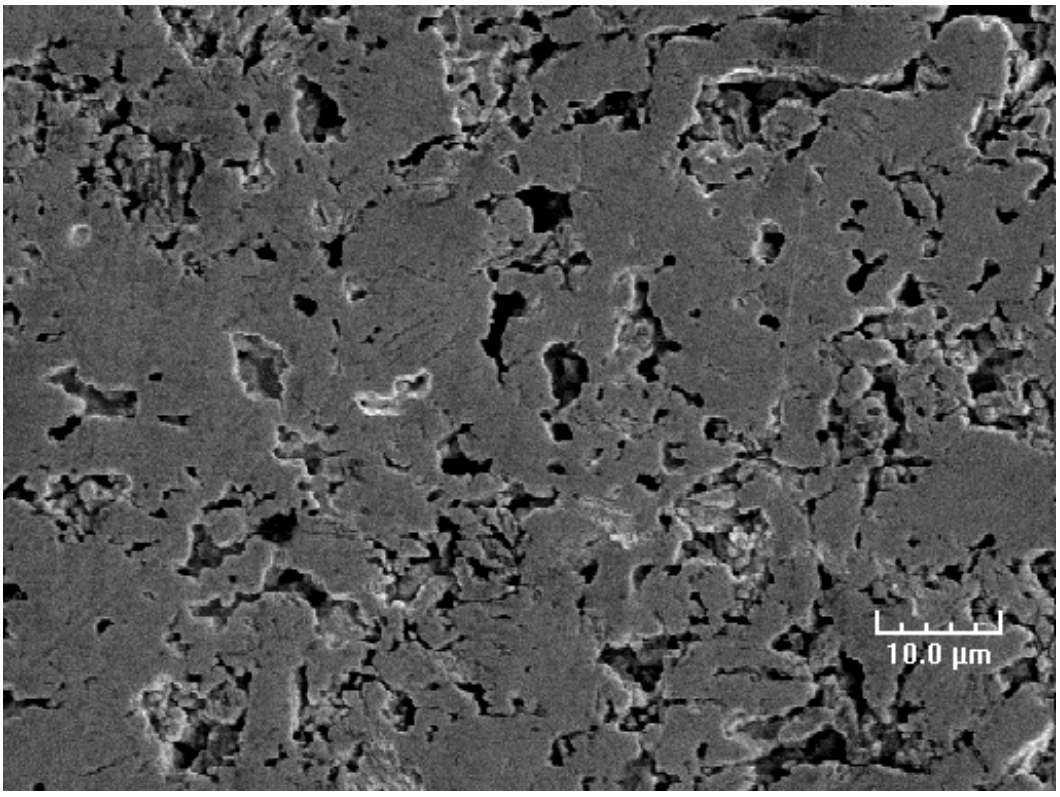

Fig. 5-1 1500X SEM image of pellet 2

Pellet 3, was 100% DU sintered at 650°C had a porosity 26 ± 2%. This porosity is significantly greater than the porosity of pellet 2. The difference in porosity is contributed to the amount of cracking in pellet 3, Fig. 5-2. The cracking was evident throughout the entirety of the pellet. The cracking is believed to be cause by the agglomeration of the particles and the non-uniform density of the pressed pellets (Section 5.2.3). There are large areas where individual particles are indistinguishable; however these areas are broken apart by large cracks and fissures. These fissures do not have the same appearance as the pores formed in other pellets. The cracks formed on different atomic planes as if a solid piece of DU was "shattered". This is indicative of the majority of the cracks forming after the pellet sintered, most likely during cool down.

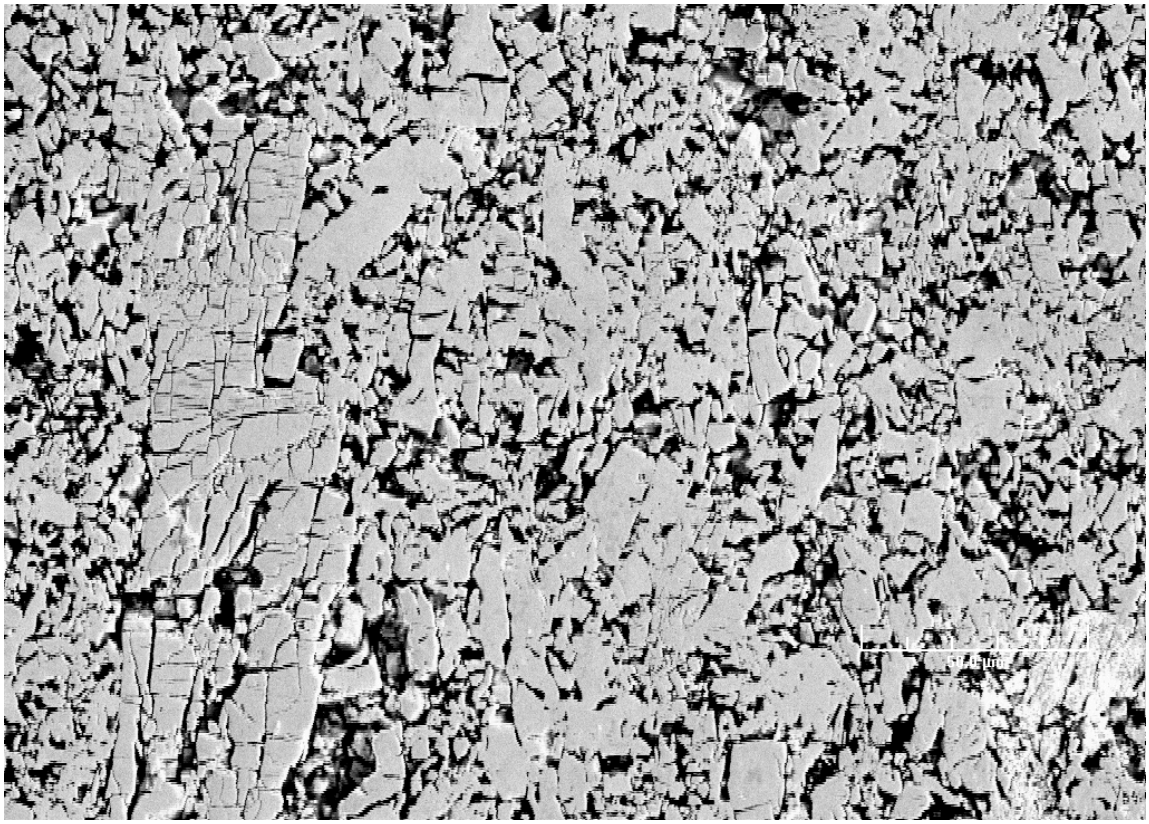

Fig. 5-2 500X SEM image of pellet 3

Pellet 5, DU-10Zr sintered at 650 and 700˚C (Table 4-1), showed visible signs of sintering. Pellet 5 had a similar porosity to that of the 100% DU Pellets 2 and 3. Once again most of the individual powder particles are no longer distinguishable. The particles have sintered and formed large grains.

There were two clear separate phases observed in Pellet 5, as seen in SEM and BSE images Figs. 5-3 and 5-4. The two phases were clearly defined in the BSE images: the light gray areas consist of DU while the dark grays consist of Zr. The Zr and DU stayed separated in the pellet and did not alloy; there was no apparent δ or γ phase. This was

confirmed through EDS of the image, Figs. 5-6 and 5-7. Six different points were chosen for EDS analysis; three points in the DU rich areas and three points in the Zr rich areas.

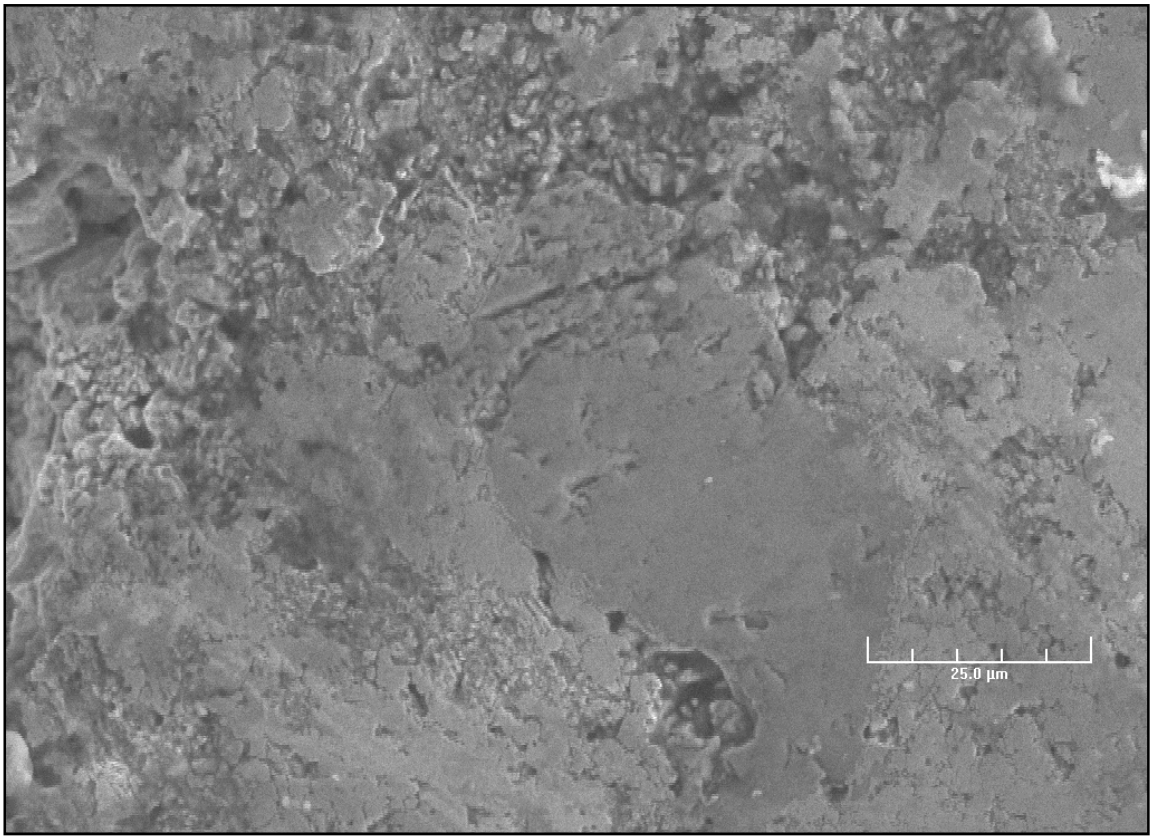

Fig. 5-3 1000X SEM image of pellet 5 (same area as Figure 5-4 and 5-5)

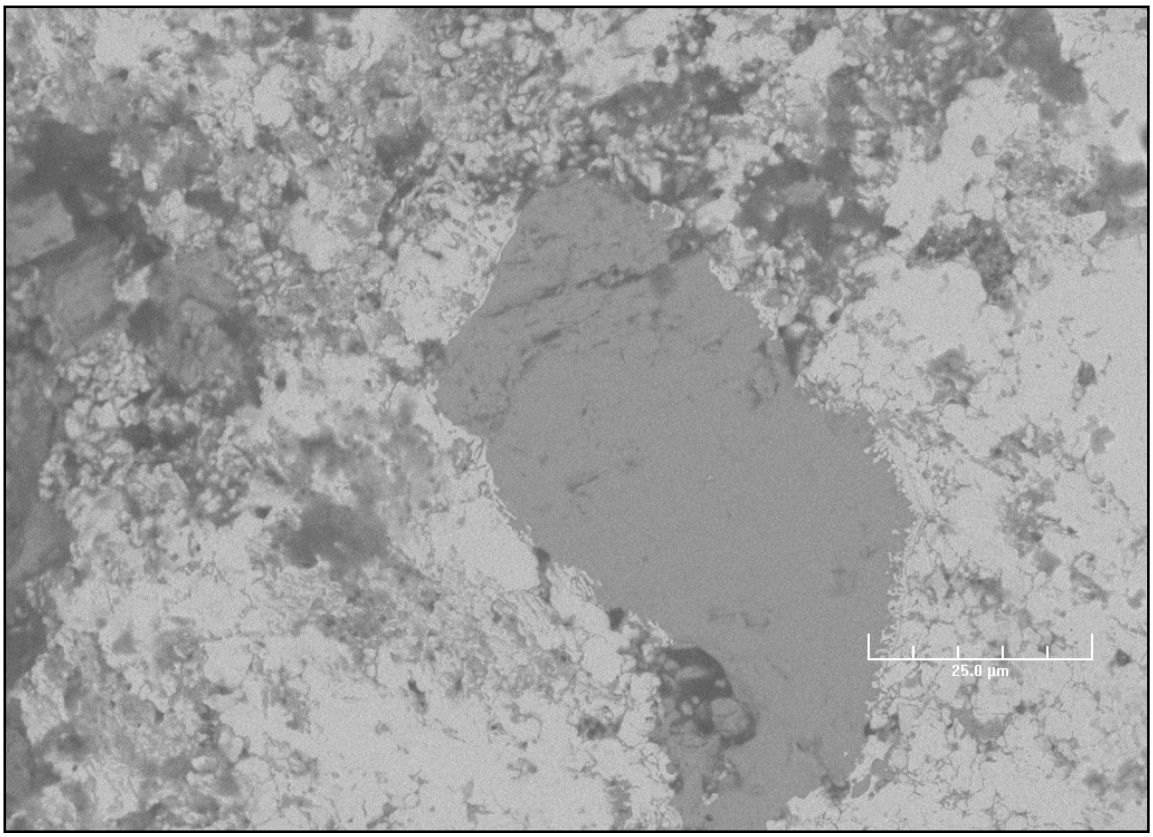

Fig. 5-4 1000X BSE image of pellet 5 (same area as Figure 5-3 and 5-5)

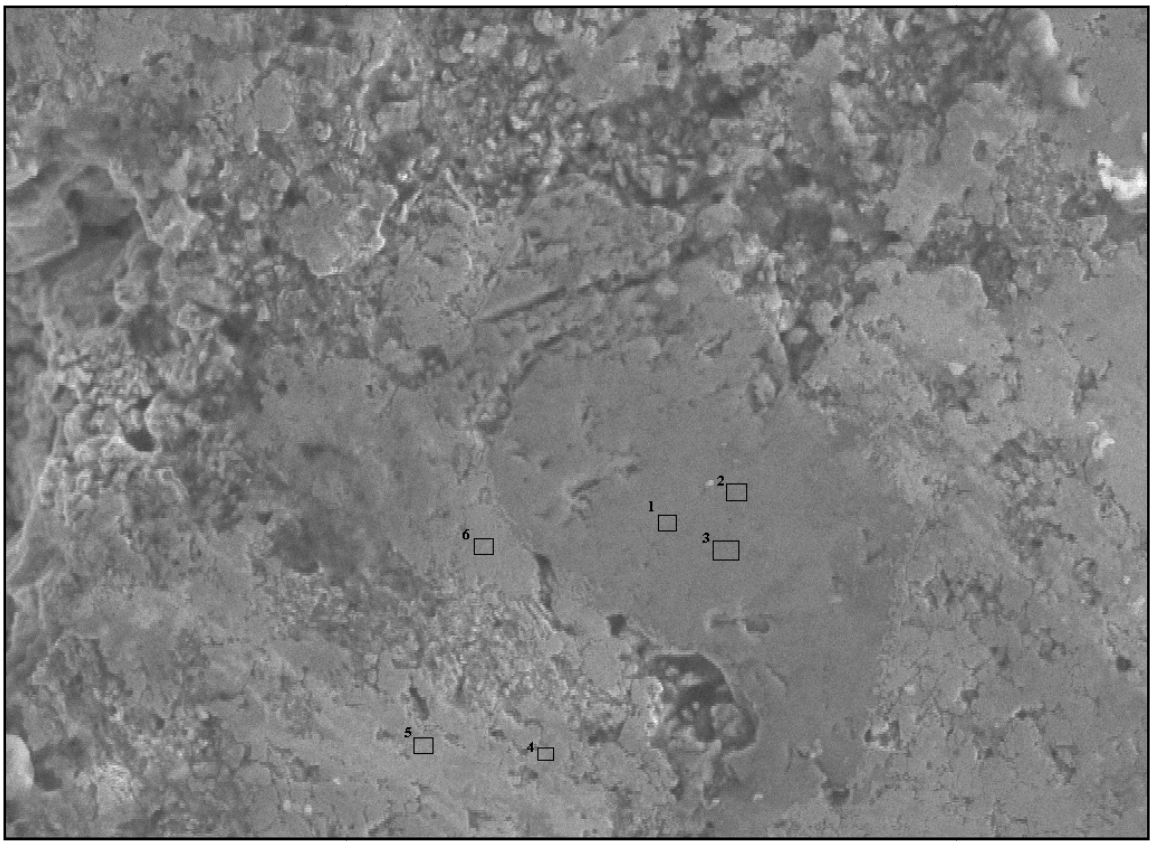

Fig. 5-5 1000X SEM image EDS map location map of pellet 5 (same area as Figure 5-3 and 5-4)

On the SEM image EDS map, Fig. 5-5, location 1 (Fig. 5-6), 2 and 3 consisted of 95.79%, 100%, and 100% Zr respectively with the remaining percentages being DU. Location 4 (Fig. 5-7), 5, and 6 consisted of 97.29%, 100%, and 99.54% DU respectively with the remaining percentages being Zr. These percentages show that a negligible amount of intermixing between the DU and Zr occurred during the sintering experiment. The separation of the U and Zr was not unexpected as most of the alloying between the two metals occurs above 865°C when both metals are in a BCC configuration.

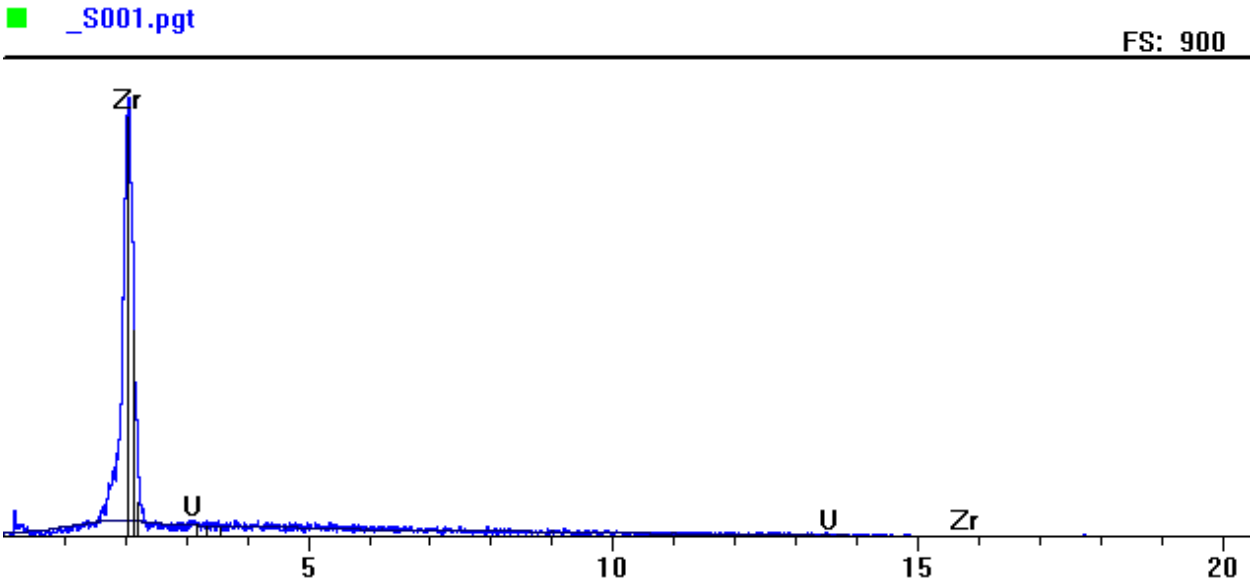

Element	Wt%	ChiSquared	Z Corr	A Corr	F Corr
Zr	95.79	7.54	0.989	1.016	1.000
U	4.21	0.50	1.307	1.264	1.000
Total	**100.00**	**0.58**			

Fig. 5-6 EDS spectrum of location 1

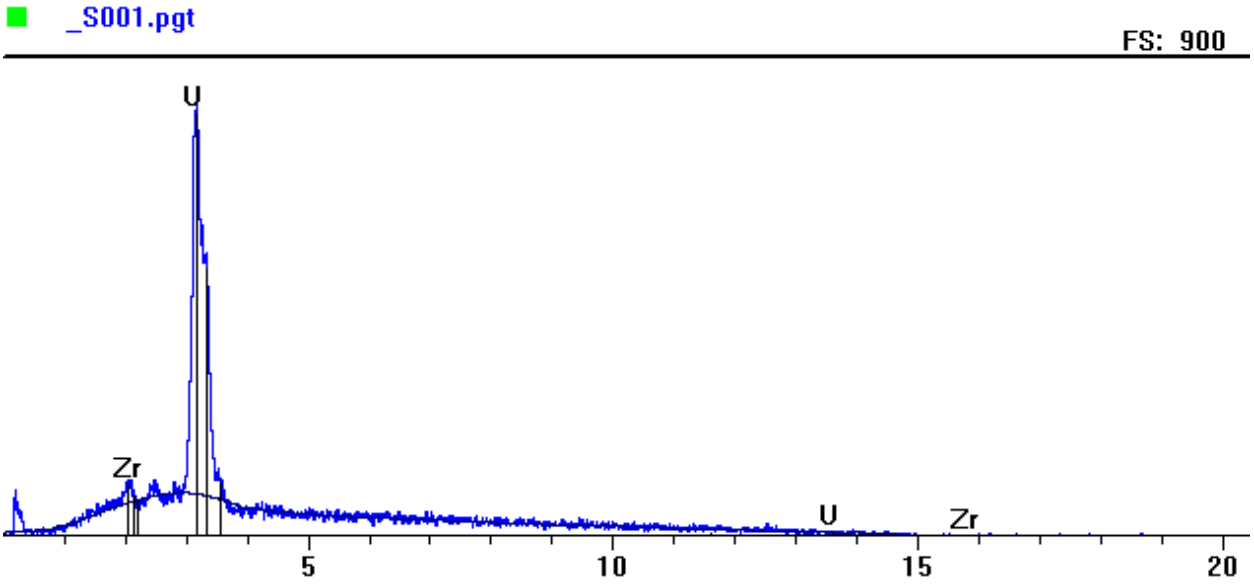

Element	Wt%	ChiSquared	Z Corr	A Corr	F Corr
Zr	2.71	0.29	0.758	1.361	1.000
U	97.29	3.12	1.009	1.007	1.000
Total	**100.00**	**0.95**			

Fig. 5-7 EDS spectrum of location 4

On lower magnification the Zr rich areas appeared to generally have less porosity than the pure DU phase of the pellet; however this is an artifact of the SEM. As the magnification was increased pores could be observed in the Zr rich areas. These pores were of a lighter color than the pores in the DU rich areas, making them more difficult to observe and account for on lower magnification settings, Fig. 5-8.

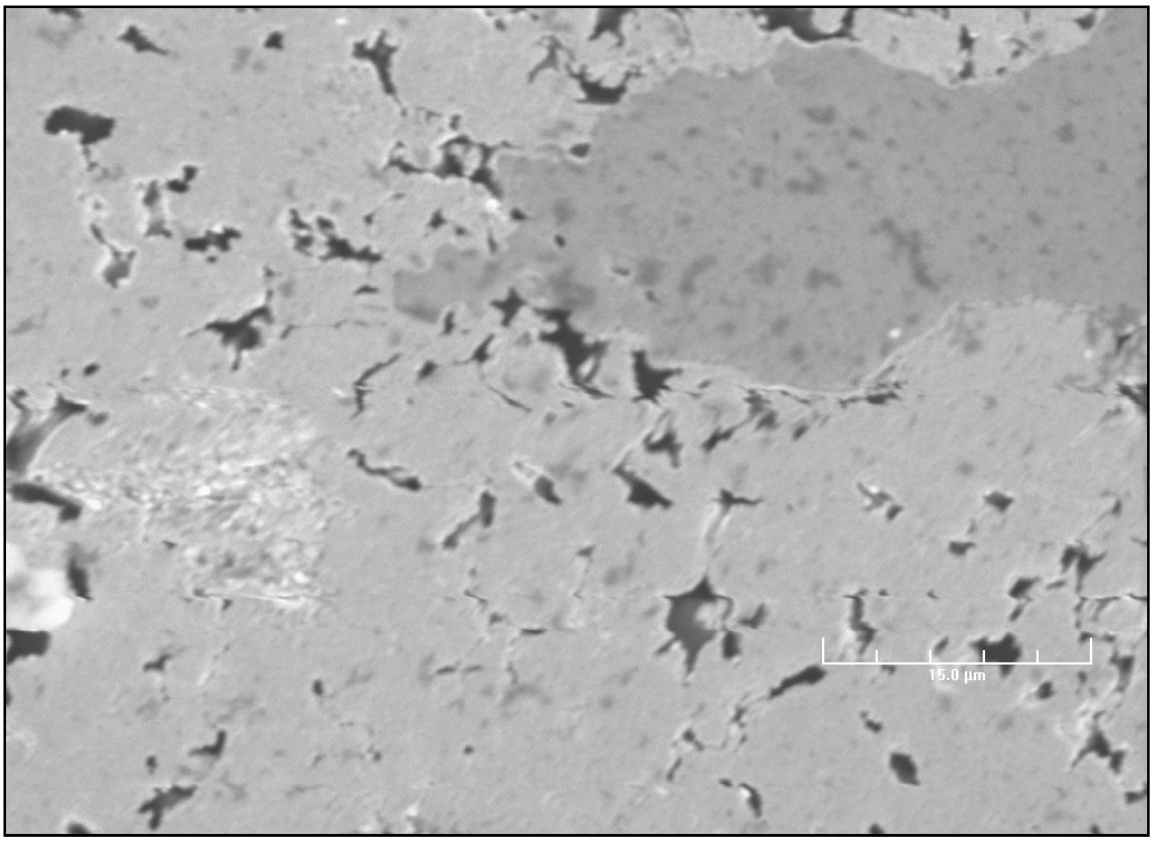

Fig. 5-8 2000X SEM image of pellet 5, the pores in the Zr rich areas are somewhat obscured

Pellet 6, DU-1Mg (wt %) sintered at 655˚C, had a porosity of 14 ± 2%. This porosity was lower than 100% DU Pellets 2 and 3 (Fig 5-9). Enhanced liquid phase sinter, due to the presence of Mg, led to the lower porosity. The images were characterized by areas with large amounts of sintering and low porosity, Fig. 5-10, and irregular shaped large pores scattered throughout the pellet, Fig. 5-11, (lengths could be greater than 25 microns).

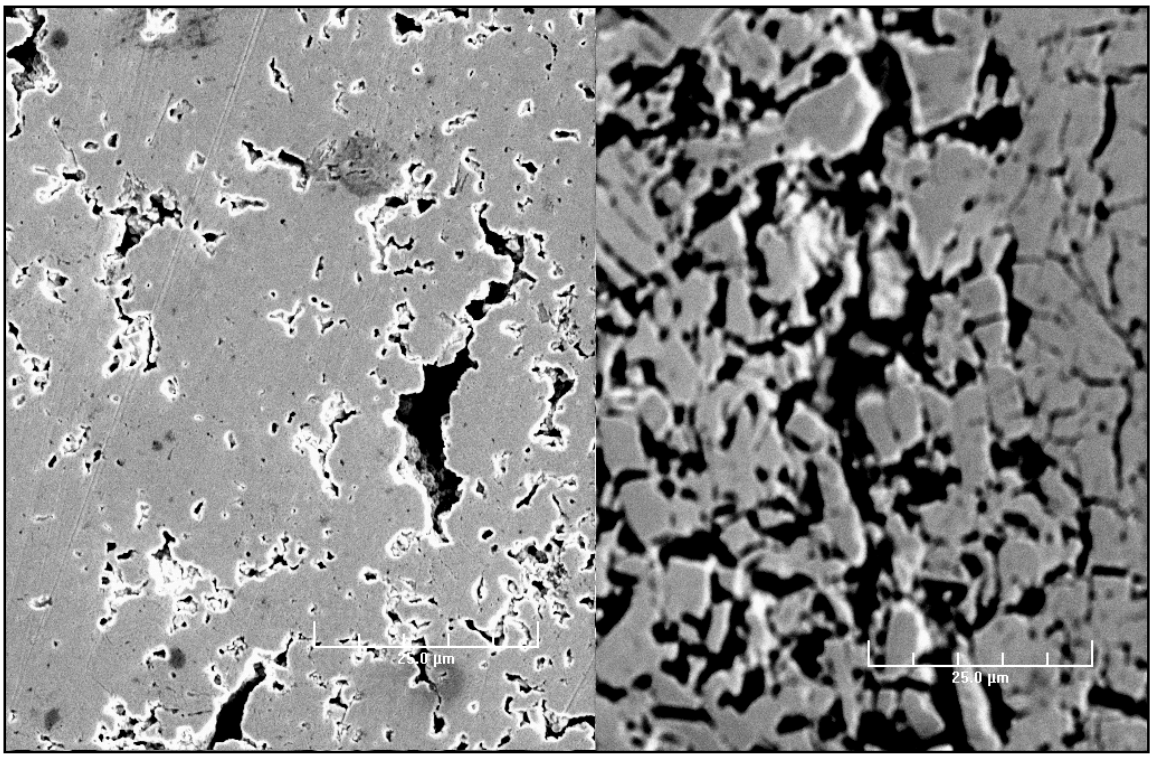

Fig. 5-9 Left 1000X SEM image Pellet 6, Right 1000X SEM image Pellet 3: Pellet 6 shows a greater amount of sintering than Pellet 3

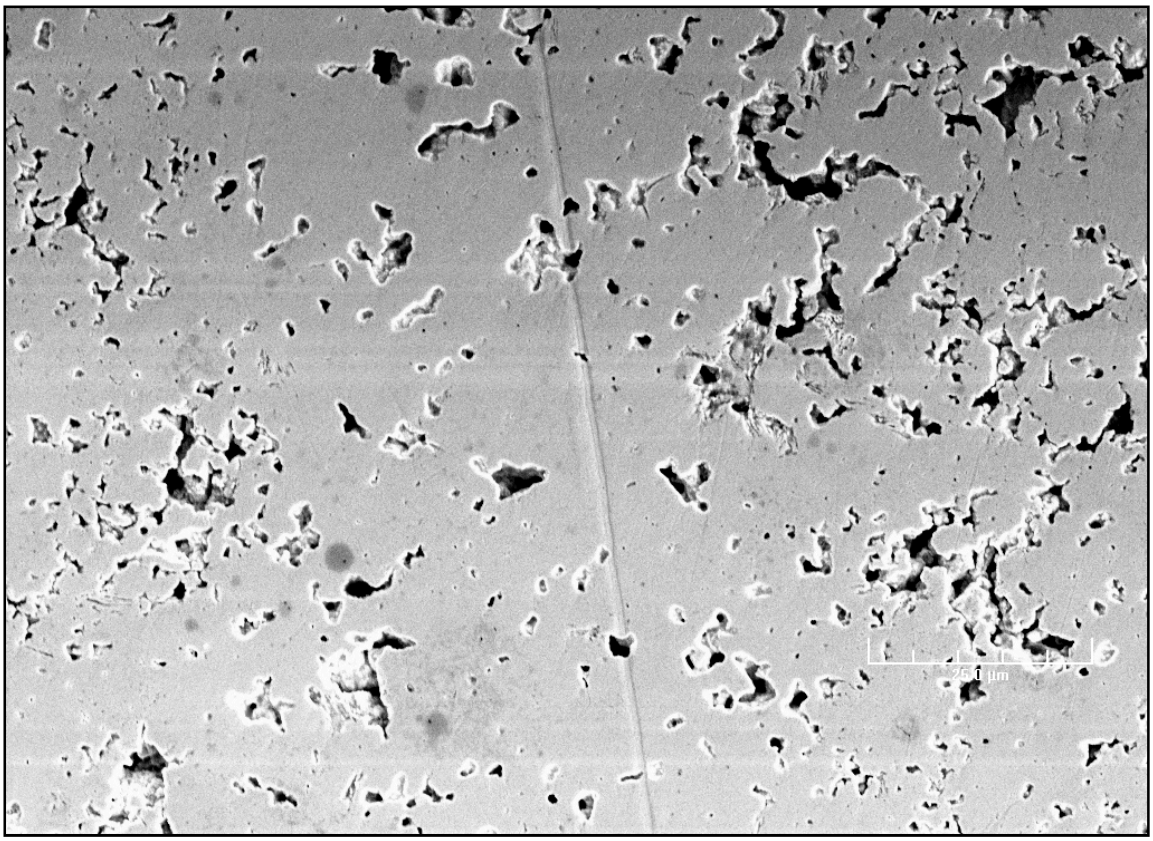

Fig. 5-10 1000X SEM image of pellet 6

Figure 5-10 shows a significant increase in sintering compared to the previous pellets. There are no grain boundaries visible and the original powder particles are not distinguishable. The increase in sintering was caused by the capillary action of the liquid Mg. There are several spherical shaped pores throughout the image along with some irregular shaped pores. There are also regions where no pores or cracking were present.

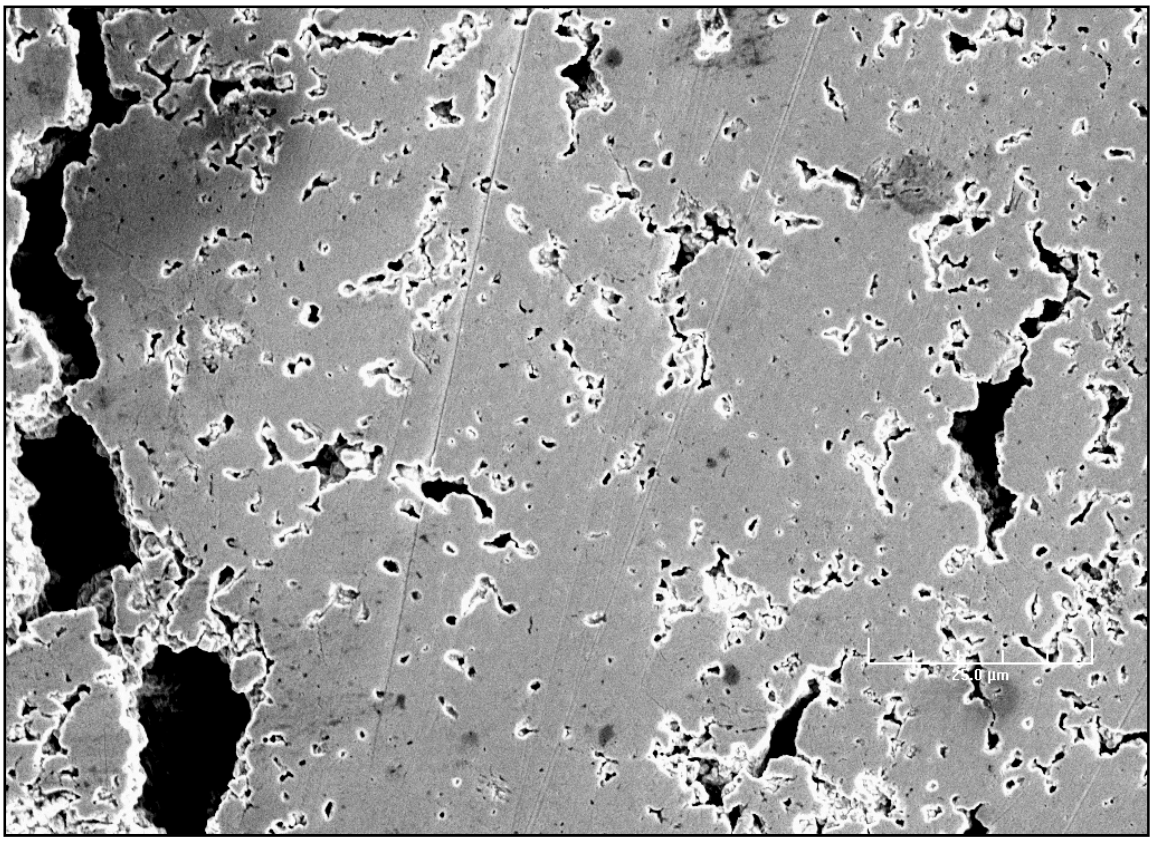

Fig. 5-11 1000X SEM image of pellet 6

Figure 5-11 contains areas of great sintering, small spherical pores, and irregular shaped pores similar in Fig. 5-10. Figure 5-11 also contains very large (greater than 25 µm) irregular pores. These large pores were consistent throughout Pellet 6 (DU-1Mg). This type of pore at this frequency was unique to Pellet 6 and not seen in the other pellets. The reason for the presence of this phenomenon in Pellet 6 is not clearly understood.

The SEM images of Pellet 10, DU-10Zr-2.4Mg sintered at 655 ˚C, show clear signs of sintering (Fig. 5-12). While there were no porosity measurements performed on Pellet 10, the porosity of the pellet was fairly low by observation. There were some small spherical

pores and some larger irregular pores. This porosity is analogous to Pellet 6, DU-1Mg, however the irregular pores in Pellet 10 were smaller and less frequent.

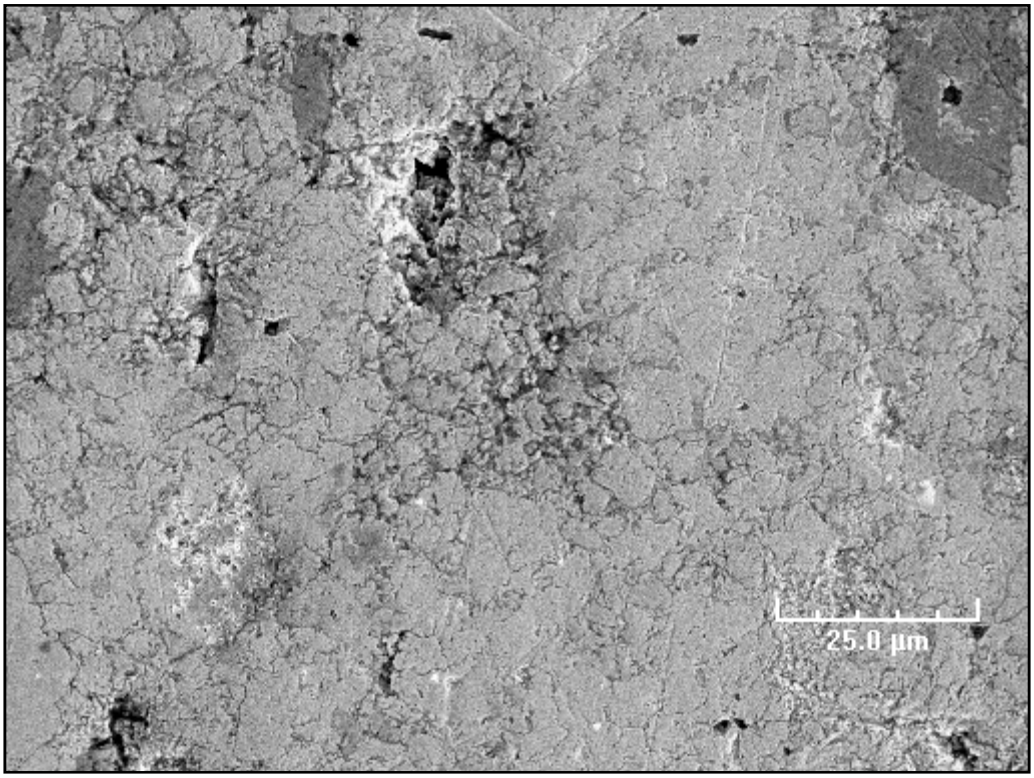

Fig. 5-12 1000X SEM image of pellet 10 (same area as figure 5-13)

There two distinct phases in the pellet. These phases can be seen in Fig. 5-13, a BSE image of the pellet, the light gray areas DU while the dark grays areas are Zr. In Pellet 10 a portion of the Zr phase gathered along the grain boundaries of the DU grains. This can be seen in Fig. 5-13 and 5-14; the dark lines between the DU grains are the Zr rich areas. The envelopment of the DU grains is attributed to the inclusion of Mg. Mg and Zr are completely soluble in each other at the sintering temperature. This solubility characteristic

combined with liquid enhanced sintering effect of the Mg caused the Zr to surround the DU grains.

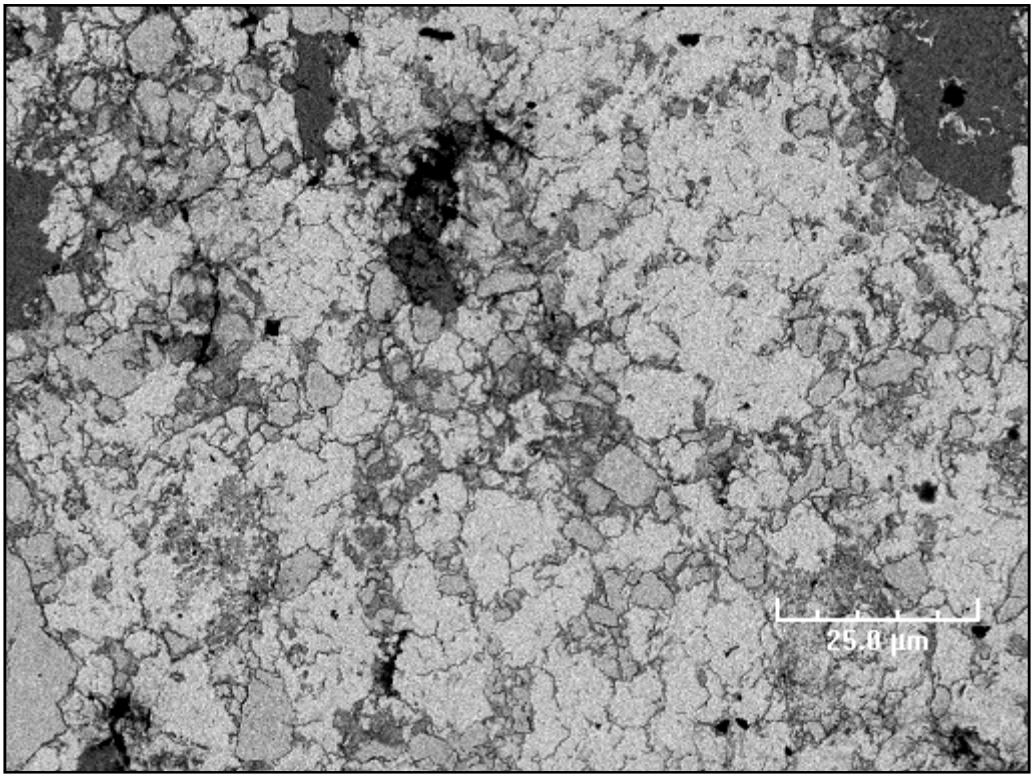

Fig. 5-13 1000X BSE of pellet 10 (same area as figure 5-12)

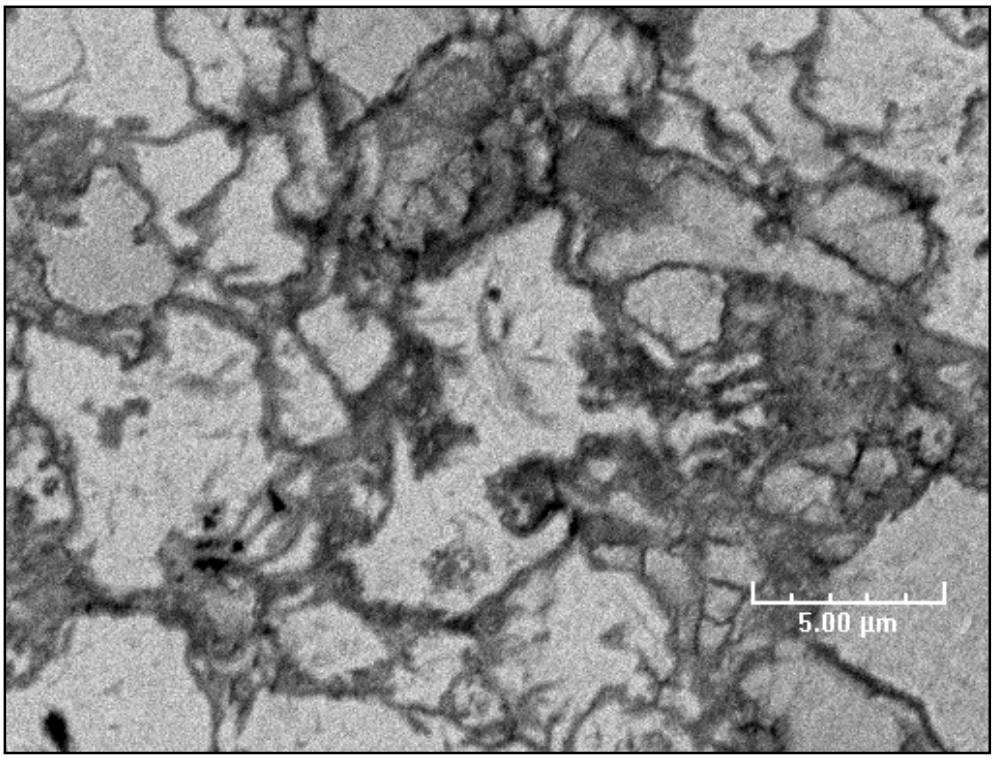

Fig. 5-14 5000X BSE image pellet 10 (close up of figure 5-15)

EDS analysis was performed on pellet 10, Figs. 5-15 through 5-17. The EDS analysis showed that the DU and Zr remained segregated. The EDS confirmed that the dark material along the grain boundaries of the DU was Zr. An EDS map is shown in Fig, 5-16. Locations 1 and 3 were in the Zr rich areas and contained 100% Zr. Figure 5-17 is a magnification of location 2 on the map. Location two consists of both the large DU grains and the surrounding Zr. This location contained 93.24 % DU, 6.76% Zr, and 0% Mg. The difficulty in detecting any significant amount of Mg in the EDS analysis can be attributed to the relative low weight percent of Mg in the pellet. There was no indication of Mg loss during the post experiment examination of the reaction vessel.

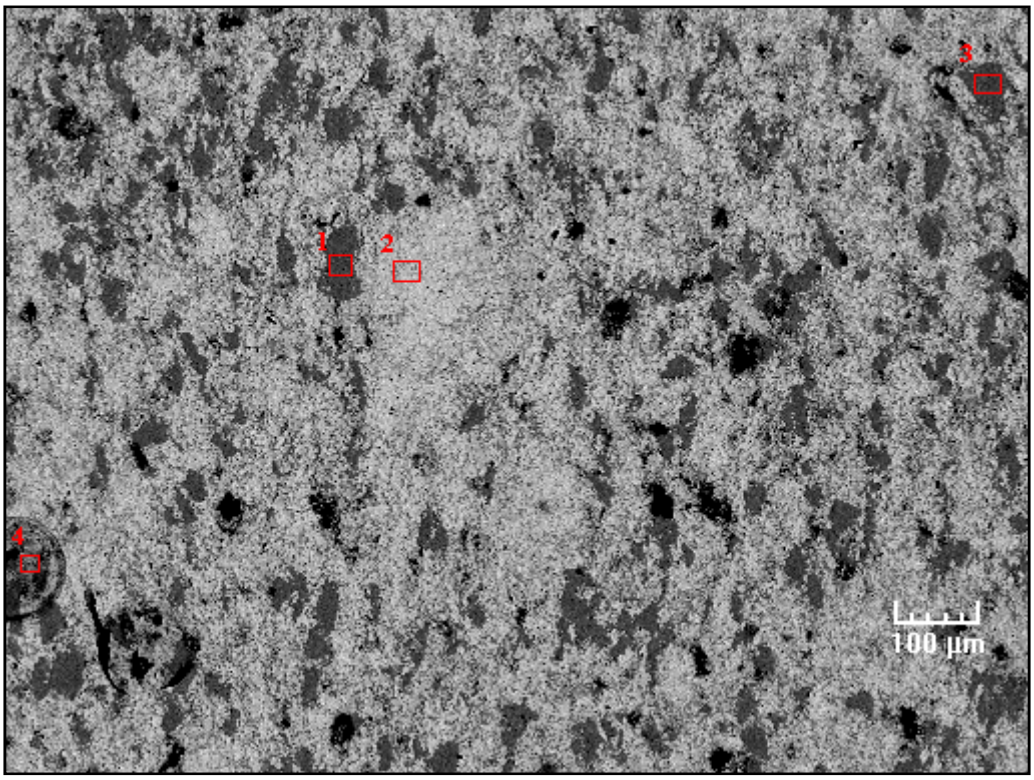

Fig. 5-15 100X BSE image EDS map

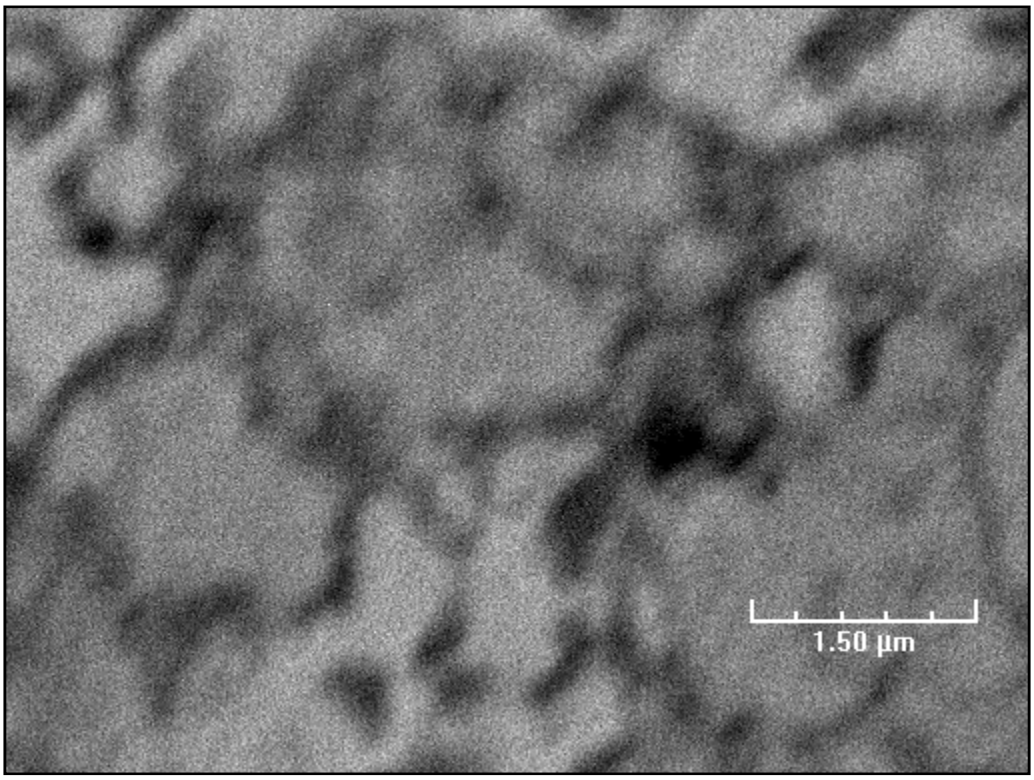

Fig. 5-16 BSE 18,000X of pellet 10 location 2

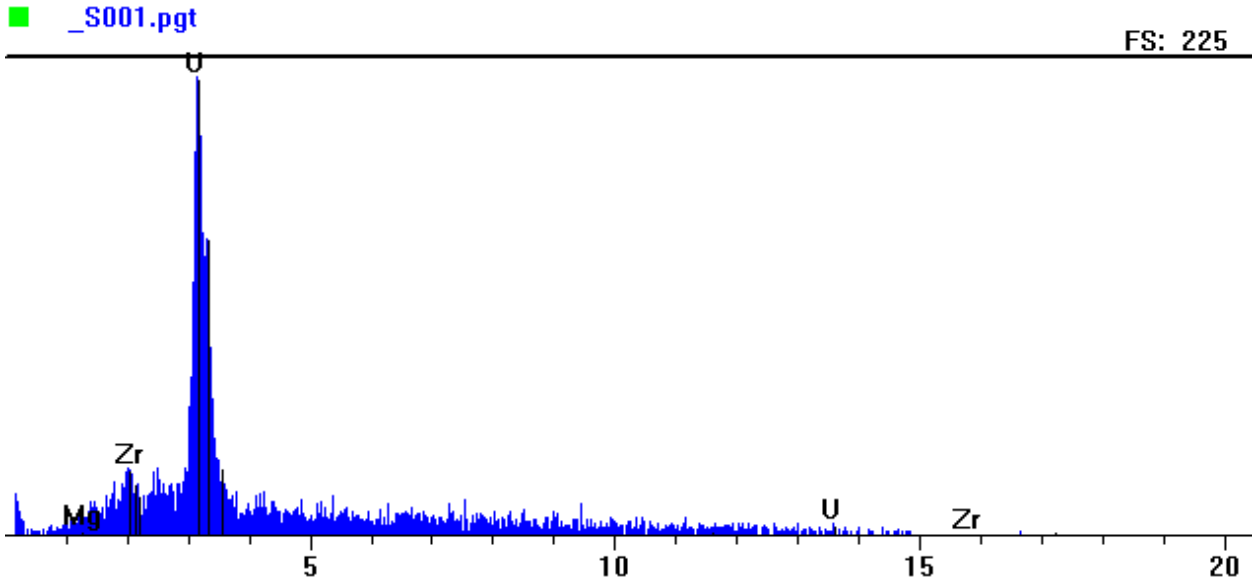

Element	Wt%	ChiSquared	Z Corr	A Corr	F Corr
U	93.24	0.67	1.022	1.018	1.000
Zr	6.76	0.90	0.769	1.347	1.000
Mg	0.00		0.578	2.502	1.000
Total	**100.00**	**0.21**			

Fig. 5-17 EDS of location 2 from Figure 5-16

5.2.3 Post Experiment Dimensional Measurements

There is a significant difference between the measured thickness of the pellet *in situ* via the LVDT and the post experiment measurements of the pellets. The LVDT data indicated a continuous shrinkage of the pellet during the sintering, while the post experiment measurements indicate an increase in the thickness of the pellet in all experiments expect experiment number 10, where there was a 0.0002 in decrease in thickness. Experiment 6 showed a slight increase in height of 0.6% and a decrease in the diameter of the pellet. While there are questions regarding the accuracy of the LVDT measurements (addressed

5.2.4), there is little doubt that the relative trends in the measurements taken by the LVDT are accurate (i.e. the pellet is shrinking along the vertical axis). The majority of the post experiment pellets, while conical shaped (addressed later in the section), do show an increase in the diameter.

The reason for the increase in thickness and diameter has not been conclusively determined, but it is believed that the cracking of the pellet during the cool down phase causes this phenomena, Fig. 5-18 and 5-19. The cracks appear mainly to be radial. The cracks were first noticed during the preparation of the pellets for SEM analysis. The cracks were initially contributed to the expansion of the pellet caused by the heat of cutting. It is appears that while the cutting of the sample exacerbated these cracks it did not cause them. The cracks appear to have formed during the cool down phase of the pellets. The effect of the cracks on the thickness of the pellets is masked during the LVDT measurements by the cool down and thermal contraction of the steel rod. It appears that the cracks could be caused by unevenly cooling of the samples or cooling the samples too quickly; the rate of cooling was approximately 5 ˚C a minute.

Agglomeration of the DU powder is another suspected cause of the cracking. Agglomeration will cause areas of varying densities throughout the pellet. These varying densities will cause differences in the rate and amount of sintering throughout the pellet. These differences can lead to the cracking of the pellet do to the internal stresses cause by this phenomenon. Another contributing factor to the cracking of the pellet could be the incomplete dehydriding of the DU powder. During the experiment, hydrogen could disassociate from any residual UH_3. The H_2 could then collect and eventually breach the pellet and be released, thus weakening the overall structure of the pellet and causing cracks.

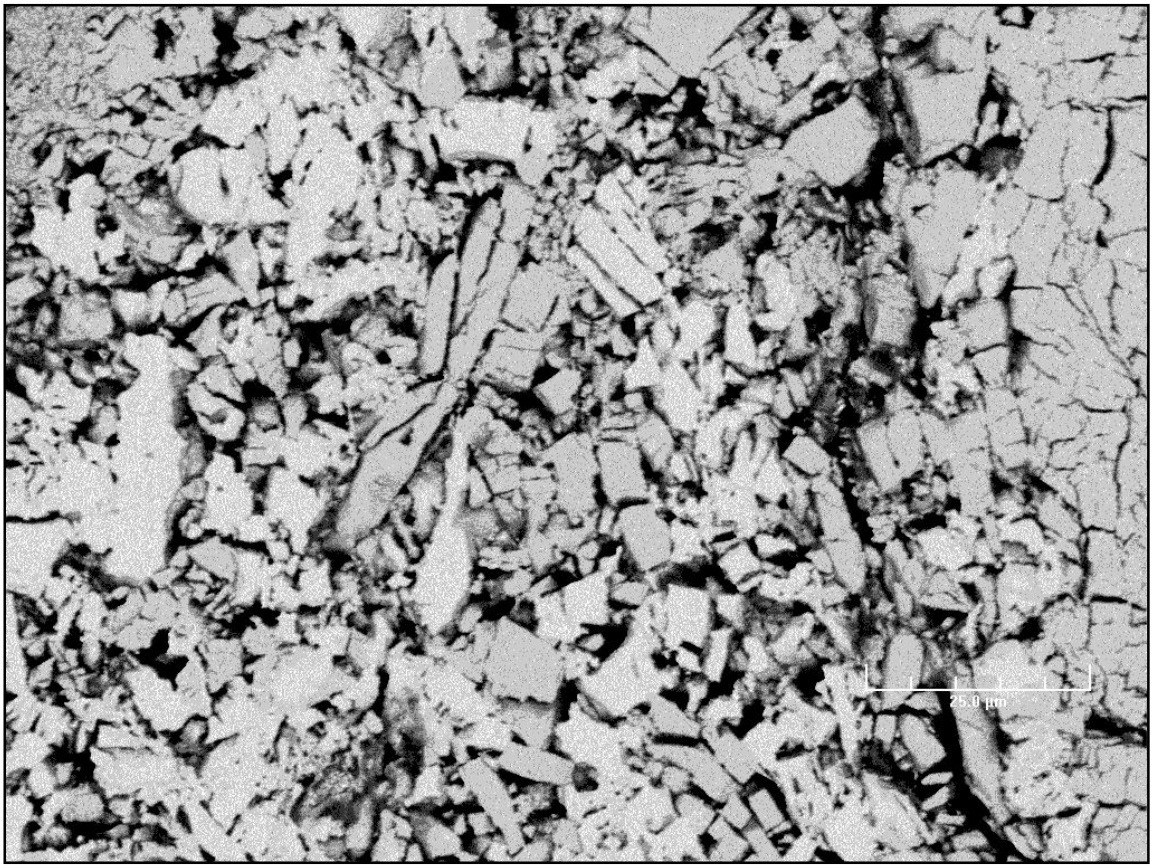

Fig. 5-18 Pellet 3 BSE 1000X visible cracks in structure

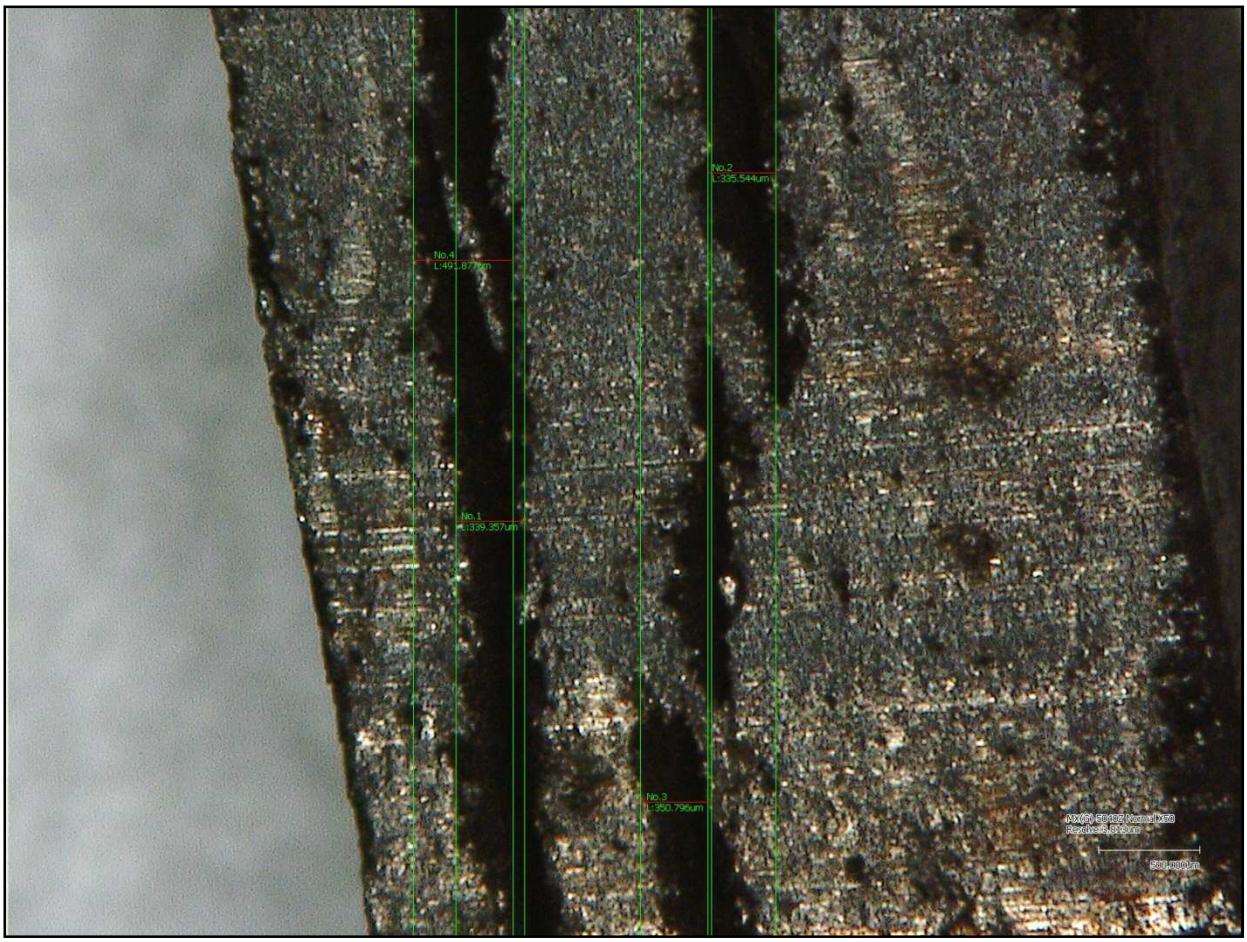

Figure 5-19 KH-1300 Image of Pellet 3

The pellets all have a slight conical post experiment shape (expect Pellet 10), with one end having a larger radius than the other. The change in shape attributed to the manner in which the pellets were pressed. When the pellets were pressed in the punch, there is a greater compaction of the powder in the lower region of the die. This leads to a higher density and lower porosity in the lower region of the pellet. With a lower porosity and higher density, there exists physical room for the pellet to compress during sintering in this region. This leads to the bottom end of the pressed pellet having a large diameter than the

top. This combined with the cracking of the pellet can give the pellet a measured increase in the post experiment diameter. Conversely, the greater porosity in the upper (pressed) region of the pellet could be a factor in the breakdown of Pellet 9. In this case the lower density portion of the pellet was placed faced down in the crucible. During the experiment the lower density region crumbled under the expansion of the pellet and weight of the LVDT measurement rod. This could also be a contributing factor to break down of the structure in Pellet 10.

5.2.4 LVDT Measurement Analysis

The LVDT provided a real time monitor of the change in pellet thickness. If one assumes the pellet shrank and swelled uniformly this can be translated into the total volume change during sintering. The LVDT was extremely sensitive to vibration or jarring of the reaction vessel during measurements. Any such action could cause a dramatic swing in voltage and skew any data taken after such a swing. Also during any ramp up or ramp down cycle the thickness change in the pellet would be loss in the expansion/contraction of the steel rod and cycling of the furnace. The data taken during a hold temperature is believed to be an accurate measurement of the thickness change of the pellet (with the possible exception of Pellet 5).

During the Pellet 4 and 8 experiment the furnace was raised to a temperature of approximately 700 ˚C, well into the temperature required for the beta phase of uranium. At this temperature the theoretical density of the uranium is 18.03 g/cm^3. and there should be a significant slowdown in the rate of sintering. The sintering rate of the pellet appeared unchanged during the hold time at the increased temperature, although most of the data at 700 ˚C is lost in the noise from the ramp up and ramp down. This would indicate that while

the thermocouple inside the crucible was at 700 ˚C the pellet did reach temperatures over 662 ˚C, the alpha beta phase transition line. During experiment 8 the furnace was raised to approximately 800˚C. At this temperature the pellet should be in the gamma phase which has a theoretical density of 18.11 g/cm^3. Also sintering of the pellet should continue in the gamma phase. However the LVDT data shows an insignificant increase in the volume of the pellet and flatting out of the shrinkage rate of the pellet. The increase could be caused by the thermal expansion of the pellet and the increased temperature or possible cracking of the pellet. The flatting of the shrinkage rate suggest that the pellet did not reach the temperature necessary to transition into the gamma phase but instead reached beta phase temperatures.

The LVDT data for pellet 4 exhibited some unexplained phenomena. After a temperature of 650 ˚C was reached there were two dramatic drops in the LVDT output voltage, Fig. 4-27. This phenomenon is believed to be caused by an error in the LVDT measurement system and not related to a change in the thickness of Pellet 4. For this reason the initial drops are not included in the $\Delta L/L$ calculation for Pellet 4.

The LVDT data for pellet 5 exhibited several rather peculiar phenomena that were not characteristic of the rest of the data obtained, Fig.4-29. There were several rapid changes in the measured pellet thickness both positive and negative. There also was a rapid increase in pellet thickness followed by a gradual decrease while the pellets temperature remained constant (650 ˚C). Also the data did not contain the immediate rapid decline followed by gradual increase in thickness during the ramp down that is characteristic of the other data collected, Fig 4-27. Instead LVDT recorded a constant thickness during the cool down period followed by a rapid decline with no gradual increase. For these reasons the

LVDT data collected for Pellet 5 is suspect however the slower rate of sintering recorded does corresponded with expected results of introducing Zr to the composition of the pellet.

6. SUMMARY AND RECOMMENDATIONS

A successful reusable system for powder production system was built. A methodology for producing fine DU powder from large chunks using the hydride/dehydride process was developed. The resulting powder from the system was pressed into a pellets of various compositions (DU, DU-10Zr, DU-Mg, DU-10Zr-Mg). These pellets were all heated to 650˚C. Some pellets were heated to 700˚C and 800˚C. The research above has laid the ground work for further experimentation and analysis of use of alpha sintering as a fuel fabrication technique.

The principle outcomes and observations from this work can be summarized as follows:

1. A successful reusable system, describe in section 3.1, was built to transform DU chunks in fine DU powder This system was used as the source of DU powder for the uranium alloy alpha phase sintering experiments.
2. The powder produced after mechanical milling was on the order of 1-3 microns in size.
3. Evidence of alpha phase sintering was observed in all of the pellets. The compositions of these pellets were: DU, DU-10Zr, DU-Mg, DU-10Zr-Mg.
4. Post experimental dimensional measurements of the pellets were found to be unreliable due to cracking during cool down.
5. The LVDT measurements were found to be extremely sensitive to outside vibrations. For this reason some the data collected was not considered to be accurate, Pellets 4 and 5.

6. The pellets of DU-10Zr showed no evidence of alloying between the Zr and DU.
7. The DU-10Zr-Mg contained large grains of DU with Zr collecting around the boundaries, Section 5.2.2.
8. The pellets had a slight conical shape post experiment. This was attributed to powder pressing procedures. During the powder pressing the density of the pressed pellet is greater on one end than the other. This leads to a gradient in the sinter rate and porosity of the green pellet and thus the conical shape post experiment.

The following observations and recommendations are presented to assist in further research in this area.

1. The rate at which the DU powder is hydrided can be increased by some or all of the following: a change to 100% H_2 process gas; an increase in the sample surface area exposed during the hydration; an increase in pressure of the process gas over the sample.
2. Oxidation of the DU powder is of the utmost concern. In order to help prevent oxidation the DU powder, the powder should be kept in an oxygen free environment and produced as needed.

REFERENCES

[1] D. E. Burkes, R.S. Fielding, and D.L. Porter, Metallic Fast Reactor Fuel Fabrication for the Global Nuclear Energy Partnership, Journal of Nuclear Materials 392 (2009), 158-163.

[2] C.E. Stevenson, The EBR-II Fuel Cycle Story, La Grange Park, Illinois: American Nuclear Society Inc. (1987).

[3] C.L. Trybus, J.E. Sanecki, S.P. Henslee, Casting of Metallic Fuel Containing Minor Actinide Additions, Journal of Nuclear Materials 204 (1993) 50-55.

[4] M.B. Waldron, B.L. Daniell, Sintering, Heyden & Son Ltd, London (1978).

[5] G.S. Udpahaya, Sintered Metallic, Ceramic Materials: Preparation, Properties and Applications, John-Wiley & Sons, Inc., Chichester (2000).

[6] R.M. German, Sintering Theory and Practice, John-Wiley & Sons, Inc., New York, (1996).

[7] J.J. Carroll, A.J. Melmed, Field Ion Microscopy of Alpha Uranium, Surface Science 116 (1982) 225-239.

[8] L. Grainger, Uranium and Thorium, George Newnes Limited, London (1958).

[9] S.F. Pugh, Swelling in Alpha Uranium due to Irradiation, Journal of Nuclear Materials 4 (2) (1961) 177-199.

[10] J.J. Burke, D.A. Colling, A.E. Gorum, J. Greenspan, Physical Metallurgy of Uranium Alloys, Brook Hill Publishing Company, Columbus (1976).

[11] W.D. Wilkinson, Uranium Metallurgy, John Wiley & Sons, Inc., New York (1962).

[12] S.M. McDeavitt (1992), Hot Isostatic Pressing of U-10Zr Alloy Nuclear Fuel by Coupled Grain boundary Diffusion and Power-Law Creep. Doctoral Thesis, Purdue University, West Lafayette, IN.

[13] S.M. McDeavitt, A.A. Solomon, Hot-Isostatic Pressing of U-10Zr by a Coupled Grain Boundary Diffusion and Creep Cavitation Mechanism, Journal of Nuclear Materials 228 (1996) 184-200.

[14] P. Chiotti, B.A. Rogers (1950), The Production of Uranium and Thorium in Powder Form, United States Atomic Energy Commission, AECD-2974.

[15] H.H. Chiswick, Advances in the Physical Metallurgy of Uranium and its Alloys, Geneva Conference Papers (1958), 713-735.

[16] C. B. Basak, R. Keswani, G.J. Prasad, H.S. Kamath, N. Prabhu, Phase Transformations in U–2 wt% Zr Alloy, Journal of Alloys and Compounds 471 (2009) 544–552.

[17] E. R. Boyko, The Structure 'of the δ Phase in the Uranium-Zirconium System, Acta Cryst. 10 (1957) 712-713.

[18] C.R. Clark, M.K. Meyer, Fuel Powder Production from Ductile Uranium Alloys, Presented at the 1998 International Meeting on Reduced Enrichment for Research and Test Reactors, Oct. 18 - 23, 1998, Sao Paulo, Brazil.

[19] T. Hashino, Y. Okijima, Mechanism of the Reaction of Hydrogen with Uranium, Journal of Physical Chemistry 77 (1973) 2236-2241.

[20] J. Bloch, The Hydriding Kinetics of Activated Uranium Powder Under Low (Near Equilibrium) Hydrogen Pressure, Journal of Alloys and Compounds 361 (2003) 130–137.

[21] A. J. Parkison (2008), Hydride Production in Zircaloy-4 as a Function of Time and Temperature, Master Thesis, Texas A&M University, College Station.

VITA

Name:	David Joseph Garnetti
Address:	Texas A&M University, 3133 TAMU, College Station, TX 77843-3133
Email Address:	dgarnetti@tamu.edu
Education:	M.S. Nuclear Engineering, Texas A&M University, 2009 B.S. Physics, Florida State University, 2005